Chem Soc Rev

REVIEW ARTICLE

View Article Online
View Journal | View Issue

Cite this: *Chem. Soc. Rev.*, 2024, **53**, 4674

Recent progress and prospects of dimer and multimer acceptors for efficient and stable polymer solar cells

Jin-Woo Lee,†[a] Jin Su Park,†[a] Hyesu Jeon,[a] Seungjin Lee,[b] Dahyun Jeong,[a] Changyeon Lee,[c] Yun-Hi Kim[d] and Bumjoon J. Kim*[a]

High power conversion efficiency (PCE) and long-term stability are essential prerequisites for the commercialization of polymer solar cells (PSCs). Small-molecule acceptors (SMAs) are core materials that have led to recent, rapid increases in the PCEs of the PSCs. However, a critical limitation of the resulting PSCs is their poor long-term stability. Blend morphology degradation from rapid diffusion of SMAs with low glass transition temperatures (T_gs) is considered the main cause of the poor long-term stability of the PSCs. The recent emergence of oligomerized SMAs (OSMAs), composed of two or more repeating SMA units (*i.e.*, dimerized and trimerized SMAs), has shown great promise in overcoming these challenges. This innovation in material design has enabled OSMA-based PSCs to reach impressive PCEs near 19% and exceptional long-term stability. In this review, we summarize the evolution of OSMAs, including their research background and recent progress in molecular design. In particular, we discuss the mechanisms for high PCE and stability of OSMA-based PSCs and suggest useful design guidelines for high-performance OSMAs. Furthermore, we reflect on the existing hurdles and future directions for OSMA materials towards achieving commercially viable PSCs with high PCEs and operational stabilities.

Received 13th October 2023

DOI: 10.1039/d3cs00895a

rsc.li/chem-soc-rev

[a] *Department of Chemical and Biomolecular Engineering, Korea Advanced Institute of Science and Technology (KAIST), Daejeon 34141, Republic of Korea. E-mail: bumjoonkim@kaist.ac.kr*
[b] *Advanced Energy Materials Research Center, Korea Research Institute of Chemical Technology (KRICT), Daejeon 34114, Republic of Korea*
[c] *School of Chemical Engineering and Materials Science, Chung-Ang University, Seoul 06974, Republic of Korea*
[d] *Department of Chemistry and RINS, Gyeongsang National University, Jinju 52828, Republic of Korea*
† These authors contributed equally to this work.

Jin-Woo Lee

Jin-Woo Lee is a Postdoctorial researcher in the Department of Chemical and Biomolecular Engineering at KAIST (2023∼). He completed his Bachelor degree at KAIST (2018) and doctorate at the same university at (2023) under the direction of Prof. Bumjoon J. Kim. His research interests include development of conjugated polymers for efficient and stable polymer solar cells as well as their wearable applications. He has published more than 50 peer-reviewed papers with H-index of 23.

Jin Su Park

Jin Su Park is a postdoctoral researcher in the Department of Chemical and Biomolecular Engineering at KAIST. He completed his BS (2017) and PhD degree (2023) at the same university, under the direction of Prof. Bumjoon J. Kim. His research interests include design and synthesis of organic semiconductors, and engineering of organic electronic devices such as polymer solar cells. He is currently working at EPFL as a postdoctoral researcher (2023∼).

1. Introduction

Polymer solar cells (PSCs) employing π-conjugated organic semiconductors as active layer materials offer distinct benefits when compared to inorganic photovoltaics (*e.g.*, silicon or perovskite solar cells) such as their light weight, transparency, and flexibility.[1–8] These advantages make PSCs promising for future electronics including wearable and portable devices. To ensure the commercial viability of PSCs, two important criteria should be satisfied: a high power conversion efficiency (PCE) of over 20% and a long-term device stability with a lifetime beyond 5 years.[9–13] The PCE of PSCs has experienced significant improvements, reaching 18–19% due to advances in various polymer donors (P_Ds) and small molecule acceptors (SMAs).[12,14–25] However, poor long-term stability of PSCs is still a significant barrier to their practical application.[26–30]

PSCs are typically divided into two categories based on the acceptor materials used in their photoactive layers: (1) SMA-based PSCs and (2) polymer acceptor (P_A)-based PSCs, also known as all-polymer solar cells (all-PSCs). In early PSC research, fullerene-based SMAs were actively investigated due to their fast and isotropic charge transport capabilities, showing a steady increase in PCEs approaching 12%.[31–34] However, these PCEs have been saturated due to the scant light absorption ability of fullerenes in the visible wavelength region. Furthermore, fullerene-based PSCs have suffered from poor long-term stability; fullerenes typically undergo dimerization and diffuse rapidly to cause phase separation in the blend film upon exposure to light and heat.[35,36] To overcome these limitations, non-fullerene SMAs have been developed.[20,21,37] Non-fullerene SMA-based PSCs have demonstrated improved PCEs, attributed to their excellent light absorption for broad wavelengths, ranging from ultraviolet (UV) to near-infrared (NIR), and high electron mobility comparable to fullerene acceptors.[20,21] Additionally, the side chains, backbones, and functional groups of non-fullerene acceptors are easily tuned compared to fullerene acceptors.[37] Initially, perylene diimide (PDI)-based non-fullerene acceptors were developed, achieving commendable PCEs of over 10%.[38–41] This was followed by the development of various SMA backbones incorporating strong dye units, pushing PCEs to exceed 18–19%, marking a significant advancement in the field of photovoltaics.[14,22–24] Nonetheless, their long-term stability has still fallen short of commercialization standards. For example, many efficient non-fullerene SMA-based PSCs have $t_{80\%}$ lifetimes (the time required for the PCE of PSCs to reach 80% of its initial value) shorter than 100 h under 1 sun illumination.[27,28,42,43] Similar to fullerenes, degradation of the optimal blend morphology is the prime factor for poor stability due to the fast diffusion of non-fullerene SMAs under external stress including light and heat. Due to the small molecular size, SMAs tend to exhibit high diffusion coefficient (D) and a low temperature onset for molecular thermal movement (*i.e.*, glass transition temperature (T_g) and cold crystallization temperature (T_{cc})), accelerating SMA diffusion and phase separation.[27,28]

The challenges related to the long-term stability of fullerene and non-fullerene SMA-based PSCs have led to a growing interest in P_A-based PSCs.[44–48] The relatively larger molecular sizes of P_As typically exhibit lower Ds and higher T_gs than SMAs, suppressing molecular diffusion and morphological deformation in photoactive layers. A number of P_As were developed utilizing naphthalene diimide (NDI) and PDI units, and their resultant all-PSCs demonstrated significantly improved light, thermal, and mechanical stabilities compared to SMA-based counterparts.[44,45,49–54] However, NDI- and PDI-based P_As possess inferior light absorption coefficients and electron mobilities compared to non-fullerene SMAs, resulting in relatively lower PCEs of below 12%. To address the performance limitations of NDI- and PDI-based all-PSCs, polymerized small-molecule acceptors (PSMAs) that incorporate high-performance SMA monomer units have been proposed.[55–60] The excellent light absorption capability and high electron mobility of SMA constituent units (*e.g.*, Y derivatives) yield PSMA-based all-PSCs with significantly improved PCEs exceeding 17–18%.[16,57,58,61–63] Furthermore, the extended chain lengths of PSMAs enable superior device stabilities upon thermal and light exposure relative to SMAs.[61,64–66] Nevertheless, the PCE of PSMA-based PSCs has lagged behind SMA-based PSCs due to the lower electron mobility of PSMAs from their irregular molecular packing and lower crystallinity of disperse PSMA materials.

Recently, discrete oligomerized SMAs (OSMAs), consisting of typically 2 to 5 SMA monomer units, have emerged as promising candidates to harness the benefits of both PSMAs and SMAs (Fig. 1). OSMAs with discrete chain lengths can be highly crystalline, yielding good electrical properties and PSCs with high PCEs. Additionally, the extended chain lengths of OSMAs exhibit significantly reduced diffusion kinetics and higher T_gs than SMAs, leading to higher device stabilities under thermal- and photo-stresses.[42,67–69] For example, the He group first demonstrated the superiority of OSMA-based PSCs in terms of PCE and stability compared to their SMA- and PSMA-based counterparts.[70] They synthesized monomer, dimer, and polymer acceptors named BTIC-EH, dBTICγ-EH, and pBTICγ-OD respectively, using the same Y SMA-based repeating backbones.

Bumjoon J. Kim

Bumjoon Kim is a Professor and Head in the Department of Chemical and Biomolecular Engineering at KAIST and he is appointed as the KAIST Endowed Chair Professor. He completed his Bachelor degree at Seoul National University (2000) and doctorate at UCSB (2006). His research interests include design of new electroactive materials for polymer solar cells with high stability and development of intrinsically-stretchable polymer solar cells. He has published more than 70 issued/pending patents and 300 peer-reviewed papers with H-index of 79.

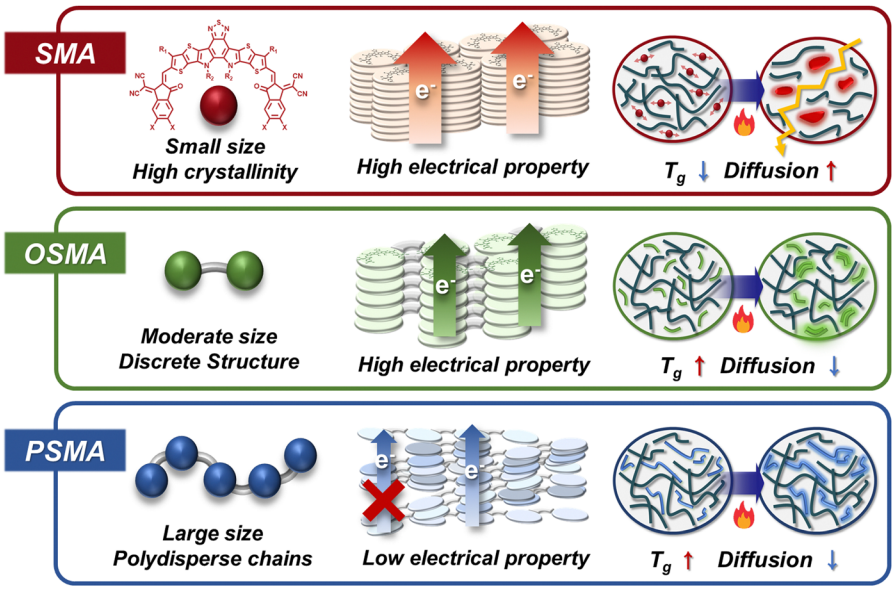

Fig. 1 Comparison in molecular configuration, electrical properties, and diffusion characteristics of SMAs, OSMAs, and PSMAs.

The PSCs based on dBTICγ-BO showed a high PCE of 16.06%, outperforming PSCs based on BTIC-EH (PCE = 10.27%) and pBTICγ-OD (PCE = 12.57%). In addition, the dBTICγ-BO-based PSCs exhibited superior photostability under 1 sun illumination with a prolonged $t_{80\%}$ lifetime of 1020 h compared to BTIC-EH- ($t_{80\%}$ lifetime = 260 h) and pBTICγ-OD-based PSCs ($t_{80\%}$ lifetime = 600 h). Subsequently, a new dimerized SMA (DSMA; 2BTP-2F-T) consisting of Y-series SMAs linked with a thiophene unit was developed by the Wei group.[71] They successfully demonstrated highly efficient PSCs with significantly enhanced PCE of 18.19%. Further advancements in OSMAs by the Huang, Li, Jen, Chen, Wang, and Kim groups have raised the PCE of OSMA-based PSCs to nearly 19%.[42,67,72–74] Moreover, these OSMA-based PSCs have shown exceptional long-term stability, with $t_{80\%}$ lifetimes surpassing 5000 h under 1 sun illumination.[67,72,73]

This young research field associated with OSMA-based PSCs shows huge potential to increase PCE and long-term stability for high performance PSCs. In this article, we review the recent exciting results of OSMA-based PSCs and provide key underlying principles that have contributed to the high PCE and enhanced stabilities of OSMA-based PSCs. This review is organized in the following order – Section 2: discussion on the historical paths to the development of OSMAs, Section 3: discussion on the design rules of recently developed OSMAs, and Section 4: discussion on the remaining challenges and outlook for the future development of OSMAs. In Section 2, we touch on conventional acceptors such as non-fullerene SMAs, P_As, and imide unit-based dimers to elucidate key design factors of oligomer-type acceptors. In Section 3, we categorize OSMAs based on core, linker, and architecture designs and summarize their relationship between structure, property, and device performance. Lastly, in Section 4, we discuss the technical limitations of OSMAs to date, directions and prospects for future development. We hope this comprehensive review will accelerate development of efficient and stable OSMAs that will eventually meet commercial standards.

2. Research background of OSMA

2.1 Development history of acceptor materials

The development of a variety of active layer materials has been key for the advancement of efficient and stable PSCs. During the last decade, important breakthroughs in the performances and stabilities of PSCs have been achieved in the transition of acceptor materials to non-fullerene SMAs and P_As, as depicted in Fig. 2. Initially, fullerene derivatives such as phenyl-C_{61}-butyric acid methyl ester ($PC_{61}BM$) and phenyl-C_{71}-butyric acid methyl ester ($PC_{71}BM$) were extensively used due to their high μ_e ($\sim 10^{-3}$ cm^2 V^{-1} s^{-1}, measured by the space-charge limited current (SCLC) method), associated with their isotropic molecular structure and strong intermolecular interactions.[31,33,75] Conventional fullerene-based PSCs achieved a maximum PCE of around 12%. However, despite chemical modifications of fullerenes, successful cases have been observed for limited systems including $PC_{61}BM$, $PC_{71}BM$, and bis-adduct type fullerene (*i.e.*, indene-C_{60} bisadduct (ICBA) and *o*-xylenyl C_{60} bisadduct (OXCBA)).[31–34,76] Importantly, the maximum PCE of fullerene-based PSCs has been saturated due to their limited light absorption capability and restricted tunability of their bandgap and energy levels. Several characteristics of fullerenes such as excessively fast diffusion coefficients, strong aggregation properties, and a tendency to dimerize by sunlight posed significant hurdles for achieving robust fullerene-based PSCs.[26,35,36]

To address the performance limitations of fullerene-based PSCs, non-fullerene SMA and P_A have been subsequently

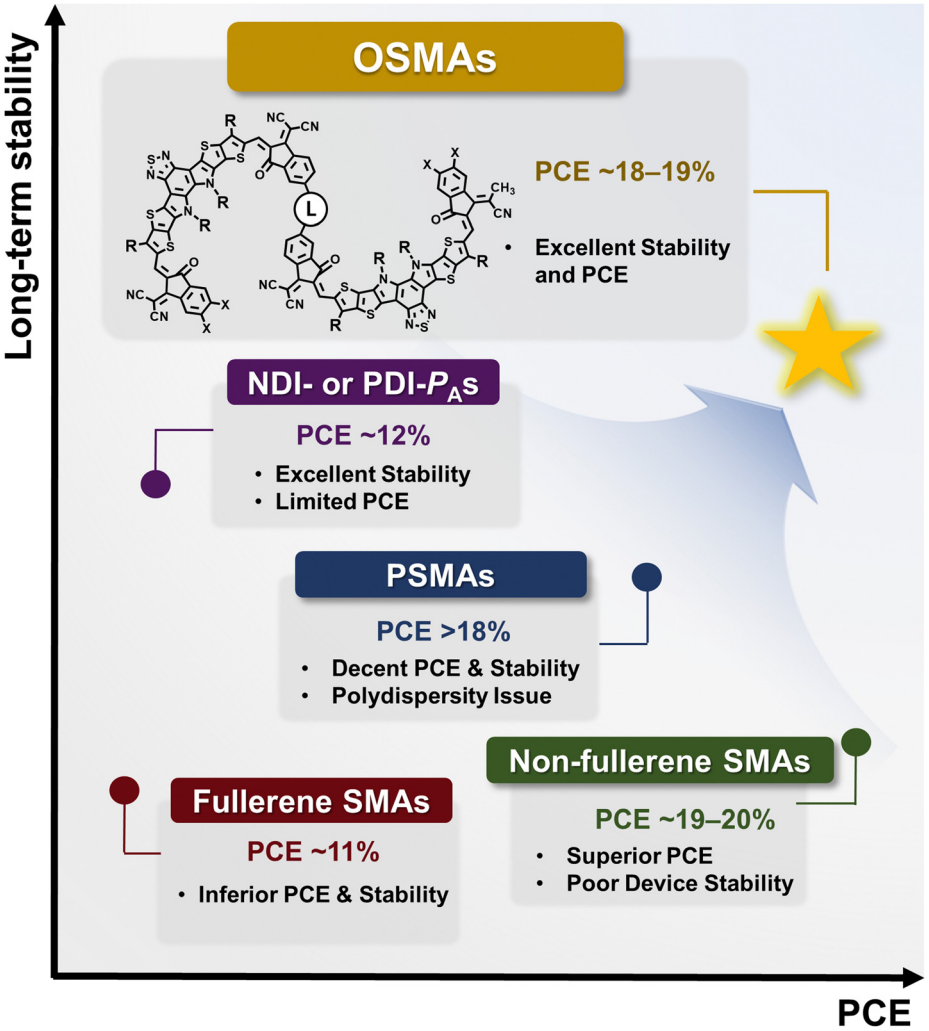

Fig. 2 Characteristics of each PSC type depending on the acceptor material.

developed.[37] First, P_A-based all-PSCs achieved remarkable device stabilities due to their mechanical robustness and morphological stability derived from long chain lengths and smaller diffusion coefficients in the films.[46,50,52,54,77–80] In particular, rylene diimide (*i.e.*, NDI and PDI) building blocks were mainly used due to their strong electron affinity and highly planar molecular structure.[47,50,81–83] Indeed, the renowned P_A (poly{[*N*,*N*′-bis(2-octyldodecyl)naphthalene-1,4,5,8-bis(dicarboximide)-2,6-diyl]-*alt*-5,5′-(2,2′-bithiophene)} (P(NDI2OD-T2)), also known as N2200), designed by Facchetti and coworkers in 2007,[47] led the renaissance of all-PSC research. In combination with suitable P_Ds, the PCE of all-PSCs increased to 11–12%, comparable to that of fullerene-based PSCs.[46,48,50] Importantly, all-PSCs demonstrated superior long-term stability compared to fullerene-based PSCs.[35,36,44,45,49] For instance, the Kim group conducted a comparative analysis between an all-PSC model (PBDTTTPD:P(NDI2HD-T)) and a fullerene-based PSC system (PBDTTTPD:$PC_{61}BM$) employing the same P_D.[35,49] Their investigations revealed that all-PSCs possessed remarkably enhanced stability against thermal, light, and mechanical stresses in contrast to fullerene-PSCs, while similar PCEs for both PSCs were achieved (6.64% for all-PSCs and 6.12% for fullerene-based PSCs). After thermal annealing for 50 h at 150 °C, the all-PSCs retained about 80% of their initial PCEs, whereas the PCE of fullerene-based PSCs dropped to 0.05% after only 5 h.[35] In addition, the all-polymer blend films had a 60 times greater stretchability of 7.16%, compared to 0.12% of the P_D:fullerene films. The superior thermal and mechanical stability of the all-PSCs is primarily attributed to the reduced diffusion kinetics and higher entanglement density of P_As with extended chain lengths compared to fullerenes.

Despite the high long-term stability of all-PSCs containing NDI or PDI-based P_As, PCEs beyond 11–12% in all-PSCs have been difficult to achieve. This is primarily due to the insufficient light absorption coefficient of NDI-based P_As, limiting the short-circuit current density (J_{sc}) of NDI-based all-PSCs. To address these issues, non-fullerene ladder-type SMAs exhibiting superior absorption and crystalline characteristics have been designed.[21,37,84–87] In 2015, the Zhan group developed

an A–D–A type non-fullerene SMA named 3,9-bis(2-methylene-(3-(1,1-dicyanomethylene)-indanone))-5,5,11,11-tetrakis(4-hexylphenyl)-dithieno[2,3-*d*:2′,3′-*d*′]-*s*-indaceno[1,2-*b*:5,6-*b*′]dithiophene (ITIC), consisting of indacenodithieno[3,2-*b*]thiophene (IDT) core and two 2-(3-oxo-2,3-dihydroinden-1-ylidene)malononitrile (IC) end groups.[88] In comparison to P_As, an ITIC SMA features excellent light absorption coefficients throughout a broad wavelength range extending to the NIR region and a higher electron mobility in the range of 10^{-3}–10^{-4} cm^2 V^{-1} s^{-1}. Building on this work, a variety of ITIC derivatives with chemically modified IDT cores, IC end-functional groups and side chains have been developed, leading to PCEs up to ~15%. In 2019, Zou *et al.* developed an enhanced SMA, specifically an A–DA′D–A-structured Y acceptor.[20] This new acceptor and its derivatives exhibit enhanced light absorption, improved crystalline characteristics, and a higher electron mobility than those of ITIC derivatives. These advantageous properties were attributed to the integration of electron-deficient aromatic rings at the central core and the substitution of cyclopentadienyls with pyrrole rings, allowing for additional electron push–pull effects along the DA′D-structured core unit that facilitate intramolecular charge transfer.[89] Moreover, the ability of Y SMAs to form 3D networks significantly improved charge mobility and J_{sc} in the resulting PSCs by providing effective charge transport channels for both electrons (*via* end-group stacking) and holes (*via* core stacking).[90,91] Therefore, the PCE of Y SMA-based PSCs has undergone a remarkable improvement, reaching a high value of over 19%.[92–94]

Despite significant advancements in the PCE of SMA-based PSCs, they still fall behind those of silicon and perovskite-based cells. The dominant factor is the relatively lower open-circuit voltage (V_{oc} < 0.9 V) of SMA-based PSCs compared to that of perovskite solar cells that often show V_{oc}s higher than 1.0 V.[95,96] Furthermore, SMA-based PSCs have poor device stabilities, mainly attributed to blend morphology degradation by the rapid diffusion of the SMA molecules.[10,26,67] To attain robust high-performance PSCs, polymerized small-molecule acceptors (PSMAs) have been actively developed by various research groups during the past few years. PSMAs consisting of multiple SMA units connected by electron-donating linkers such as thiophene, selenophene, or benzodithiophene exhibit upshifted lowest unoccupied molecular orbital (LUMO) energy levels compared to SMAs, allowing all-PSCs to have a higher V_{oc} (>0.9 V).[16,61–63,97,98] In addition, the larger molecular sizes of PSMA-based all-PSCs yield much greater long-term stability against thermal and light exposures as well as mechanical stresses.[57,62,64–66,97,99–101]

The first PSMA named PZ1 was developed by the Li group.[56] They polymerized IDIC-C16 SMAs using electron-donating thiophene linkers. Subsequently, several IDIC- or Y-based PSMAs have been developed by modifying their core structures, side chains, and terminal groups.[55,57–59,65,102] For instance, the Wang group developed a series of IDIC-based PSMAs (*i.e.*, PF2-DTC, PF2-DTSi, and PF2-DTGe) by altering the bridging atoms in the linkers (C, Si, and Ge, respectively).[65] They demonstrated that PF2-DTSi based all-PSCs had a higher PCE (10.77%) and superior stretchability (crack-onset strain (COS) = 8.6%) than SMA derived PSCs with the same core unit (IDIC16, PCE = 4.93% and COS = 1.4%). Additionally, the Kim group synthesized a series of Y-based PSMAs known as P(BDT2BOY5-X) (X = H, F, and Cl), modifying the halogen atoms on the benzodithiophene linkers.[64] They demonstrated superior PCE (10.67%), stretchability (COS = 15.9%), and thermal stability, outperforming their SMA-based counterparts (Y5-2BO, PCE = 6.91% and COS = 2.3%). By virtue of the contributions from different research groups, the PCEs of all-PSCs have now increased to over 18% by engineering their backbone, side chains, linker structures, and regioregularity in PSMAs.[16,61,101,103–108]

Nevertheless, the PCE of PSMA-based all-PSCs still falls short of the state-of-the-art SMA-based PSCs (PCE ~ 19–20%). The relatively lower PCEs of all-PSCs are associated with insufficient electron mobility of PSMAs and suboptimal blend morphologies of the all-polymer blend films. The longer and polydisperse chains of the PSMAs compared to SMAs result in disordered intermolecular assemblies and lower crystallinity, thereby decreasing electron mobility of PSMAs. Furthermore, batch-to-batch variations in disperse PSMAs present a challenge in the scalable and reproducible fabrication of all-PSCs. Importantly, most high-performance PSMA-based all-PSCs have employed PSMAs with number-average molecular weights less than 10–15 kg mol^{-1}, limiting their thermal stability and mechanical robustness, which is strongly dependent on molecular weight (MW).

Discrete OSMAs, which contain a precise number of SMA monomers ranging from 2 to 5, have recently gained great interest. These oligomer acceptors retain high stability in PSCs due to their sufficient chain length, imparting higher T_gs and lower Ds than their SMA counterparts.[42,68,72–74] Moreover, the integration of electron donating linkers in OSMAs can increase the LUMO energy level compared to that of the SMAs, thereby achieving a higher V_{oc} in the PSCs.[42,71,73] Simultaneously, the discrete molecular structure of OSMAs enables them to form strong intermolecular assemblies and crystalline structures, affording excellent electron mobility in films.[67,70] Therefore, discrete OSMAs represent an effective molecular structure that successfully leverages the benefits of SMAs and PSMAs. These advantages have led to recent successful examples of the Y-based DSMAs and OSMAs.[42,72,73,109]

Fig. 3 summarizes the progress in photovoltaic performance of PSCs using different types of dimer and multimer acceptors during the past years. The concept was first explored in the PDI-based cores to develop PDI dimer and multimers in the early 2010s.[41,110,111] Although the molecular structures of PDI-based dimers and multimers are different from recent Y-molecule based OSMAs in various aspects including molecular structures, properties, and photovoltaic performances, many lessons from the PDI-based acceptors offer valuable insights into the design of current high-performance (PCE > 18%) OSMAs. In the next section, we first delve into the molecular design principles of PDI-based dimer and multimer acceptors and discuss the relationship between the molecular structure, molecular property, and PSC performance. Then, we will move

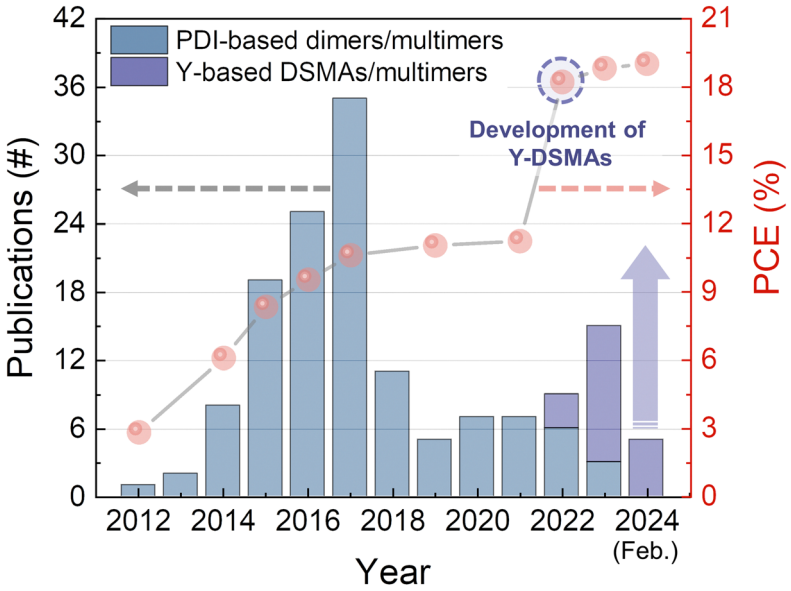

Fig. 3 Progress in photovoltaic performances of PSCs based on PDI- and Y-based oligomer acceptors during the past years.

to a discussion on the development process of OSMAs in the section thereafter.

2.2 General design rules for PDI dimers and multimers

Dimer acceptors were first designed for PDI-based acceptors (Fig. 4). PDI units were considered to be promising n-type building blocks due to their outstanding electron-accepting ability, high electron mobility through planar π-conjugation, and facile energy-level tunability by chemical functionalization. A crucial concern related to monomer-type PDI acceptors was their severe aggregation from their highly planar backbone and strong π–π intermolecular interactions, resulting in very low solubility in common processing solvents. Aggregated PDI molecules and their resulting phase-separated blend morphologies with P_Ds limit charge generation and collection, producing low PCEs in the PDI-based PSCs. Thus, alleviating the planarity of PDI acceptors through molecular engineering is a rational approach to prevent large PDI aggregates in the active layer. For example, two PDI building blocks can be combined by a linker capable of distorting the dihedral angles between the different PDI units and reducing the overall molecular planarity. Indeed, it was observed that PDI dimers with tuned molecular planarity exhibited enhanced processability and improved blend morphologies with P_Ds with increased intermixed domains.[41,88,110] Subsequently, this concept has been successfully extended to produce PDI-based trimers and tetramers.[112–115] Despite these efforts, there were still limitations to optimize the photovoltaic performances of the PDI-based acceptors. For example, the outstanding electron-transport capability of the acceptors was frequently compromised due to the decreased crystallinity upon distorting PDI backbones. Thus, one of the primary objectives of PDI dimer or multimer design was to balance the trade-off between their solubilities and crystallinities. To accomplish this, the careful consideration of linkers connecting two and more PDI units in PDI dimers and multimers is necessary to effectively regulate the molecular planarity and the resulting properties of PDI acceptors.

2.3 PDI-based dimer acceptors

The primary distinction between PDI dimers and their monomer counterparts is the presence of linkers that connect the PDI units (Fig. 5). The PDI dimers are classified into *bay-*, *imide-*, *ortho-*, and *fused-linked* types according to their linker positions. The location of linkers plays a pivotal role in determining the backbone conformation, intermolecular interactions, and overall crystallinity of PDI dimers. In this section, we provide examples of PDI dimers from the past and discuss the relationship between the chemical structures, molecular properties, and photovoltaic performance of the resulting PSCs. We also focus on describing important design principles for the PDI-based dimer acceptors. Thus, for comprehensive advances in the PDI-based dimers, we refer readers to Tables reported in other excellent reviews.[116–119]

Narayan group first demonstrated the potential of a dimerization approach by developing a PDI dimer coupled by a single bond at the imide position (Per1).[120] A PCE of 2.78% was achieved in the PSCs based on Per1, in stark contrast to a PCE of 0.13% in those with the monomeric PDI analog. The improvement was mainly attributed to decreased aggregation of Per1 and the resulting uniform blend morphology due to steric hindrance between PDI units with a twisted backbone conformation. Similarly, Yao group developed a PDI dimer connected by a thiophene linker (Bis-PDI-T-EG), which exhibited a large torsion between the PDI units with a dihedral angle greater than 50°.[110] The PCE of PSCs based on the Bis-PDI-T-EG was 4.03%, surpassing that (0.13%) of the analogous monomer-based PSCs. Therefore, the early studies on PDI dimers primarily aimed to enhance torsion between PDI units to ensure

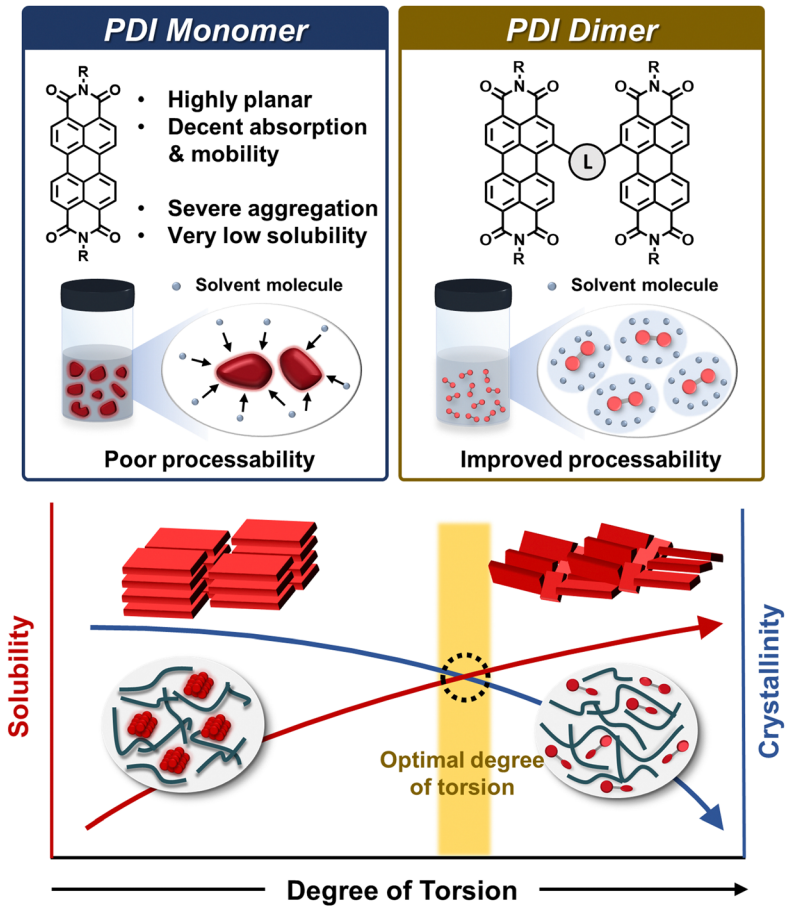

Fig. 4 General design rules for achieving PDI dimers and multimers with balanced solubilities and aggregation properties through tuning molecular planarity.

solution processability of the dimer acceptors by preventing excessive aggregation.

Nevertheless, limitations to optimizing the molecular properties and photovoltaic performances persisted: excessive distortion in the PDI dimer backbone resulted in substantial deterioration of their optical and electrical properties and lowered the PCE of the PSCs. Thus, researchers investigated the optimal molecular conformation and planarity of PDI dimers to achieve both sufficient solution processability and high photovoltaic performance. For example, Zhan group developed a range of PDI dimers, P*n*TP (n = 0–3), bridged by oligothiophenes comprising different numbers of thiophene units (Fig. 5a).[121] As the number of thiophene units increased from 0 to 3, PDI dimer backbone became progressively more planar, as evidenced by the dihedral angle between the PDI units reduced from 62.7° to 50.7°. Interestingly, the single thiophene linker (P1TP), exhibited the best PCE of 3.61% among the PSC series. The high PCE of P1TP-based PSCs was attributed to its balanced processability and aggregation properties from the appropriate linker flexibility. In addition, Xiao group developed three distinct PDI dimers with different aggregation and crystalline properties by adjusting the linker position (*bay*-to-*bay*: *bb*-2PDI; *ortho*-to-*ortho*: *oo*-2PDI; and *bay*-to-*ortho*: *bo*-2PDI) (Fig. 5b).[122] While all three dimers had adequate solution processability, the *oo*-2PDI backbone was the most planar among the series. Thus, its electron mobility was significantly higher (5.7×10^{-5} cm^2 V^{-1} s^{-1}) than those of *bb*-2PDI (2.2×10^{-5} cm^2 V^{-1} s^{-1}) and *bo*-2PDI (1.5×10^{-5} cm^2 V^{-1} s^{-1}). As a consequence, the PCE of *oo*-2PDI-based PSCs (8.30%) was greater than that of *bb*-2PDI- (PCE = 6.41%) and *bo*-2PDI-based PSCs (PCE = 2.01%).

Subsequent efforts focused on fine-tuning the molecular structures of PDI dimers to enhance their electron mobility, optimize blend morphology, and improve energetics relative to P_D. For example, Jen group developed three fully-fused PDI dimers with high electron mobilities.[123] Each PDI dimer was tethered with different linkers such as furan (FPDI-O), thiophene (FPDI-T), and selenophene (FPDI-Se), respectively (Fig. 5c). It was reported that FPDI-T, which exhibited the highest crystallinity and electron mobility, produced the best PCE of 6.72% among series. Notably, the performance of FPDI-T-based PSCs surpassed that of the non-fused thiophene-linked PDI dimer (PDI-T, PCE = 3.68%), owing to orders of magnitude higher electron mobility of FPDI-T (1.6×10^{-4} cm^2 V^{-1} s^{-1}) compared to that of PDI-T (1.4×10^{-6} cm^2 V^{-1} s^{-1}). In addition, Yan group developed a PDI dimer (SF-PDI$_2$) with a high-lying LUMO energy level using an electron-donating spirobifluorene (SF) linker (Fig. 5d).[124] The goal of this design was to improve the V_{oc} of the PSCs. The resultant PSCs not only exhibited an impressive PCE of 9.5% but also a remarkable V_{oc} of 1.11 V.

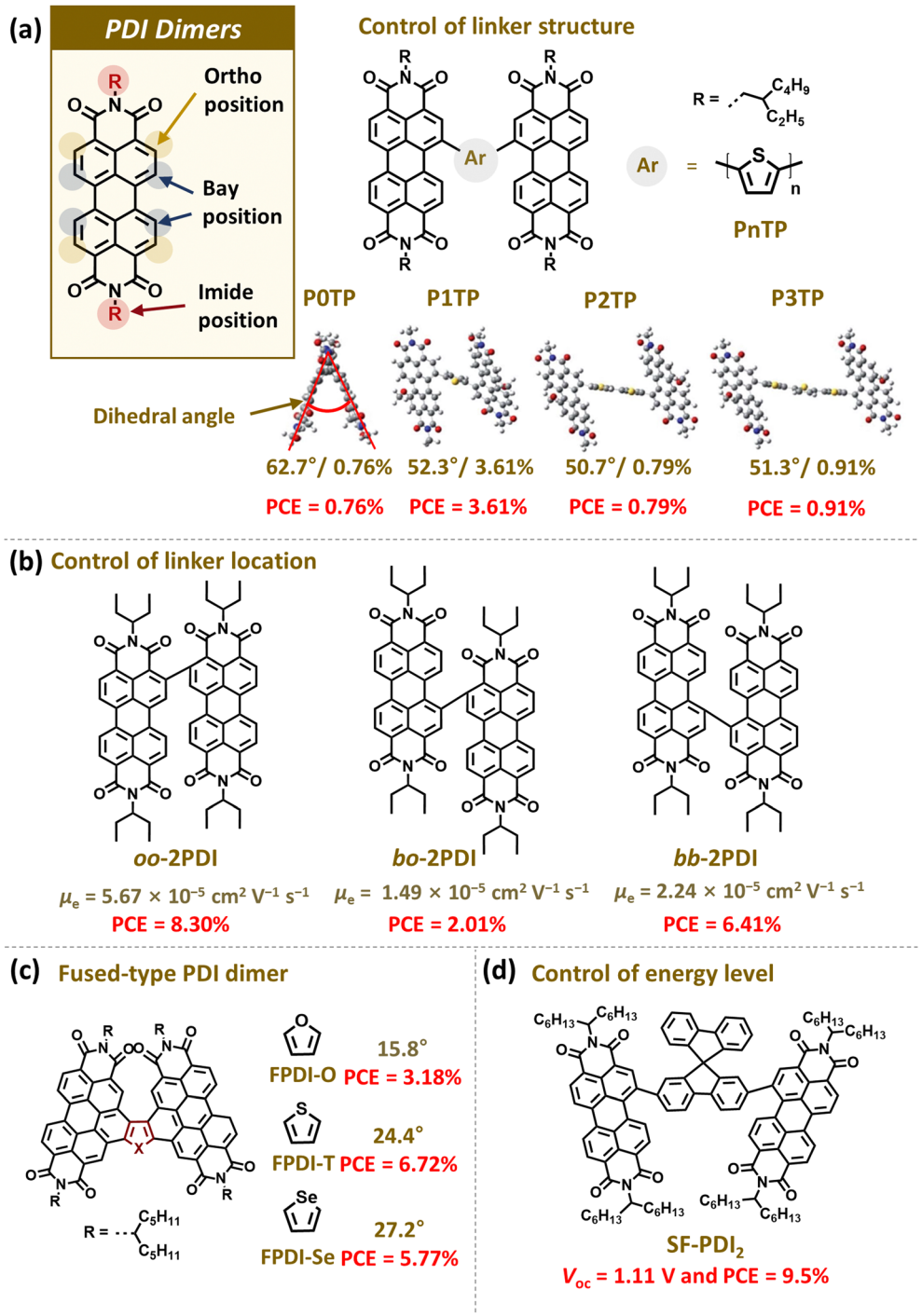

Fig. 5 Representative examples of PDI-based dimer acceptors; (a) P0TP, P1TP, P2TP, and P3TP, (b) *oo*-2PDI, *bo*-2PDI, and *bb*-2PDI, (c) FPDI-O, FPDI-T, and FDPI-Se, and (d) SF-PDI_2. Reproduced from ref. 121 with permission from the Royal Society of Chemistry, copyright 2024.

Later, the PCE of PDI dimers-based PSCs surpassed the PCE threshold of 10% because of various molecular engineering of PDI dimers.

2.4 PDI-based multimers (trimer, tetramer, and others)

Beyond the dimerization of PDI units, the sequential connection of multiple PDI repeating units has been achieved to construct PDI multimers. The extension of π-conjugation and formation of 3D or quasi-3D molecular structures with PDI multimers can further enhance the PCE of the resulting PSCs. PDI multimers can be classified into linear and star-shaped types depending on their molecular conformation (Fig. 6 and Table 1). As an example of linear PDI multimers, Nuckolls group developed helical PDI trimers (hPDI3) and tetramers (hPDI4) by the ring fusion of PDI blocks at the bay position.[125] Despite their relatively large molecular sizes, their

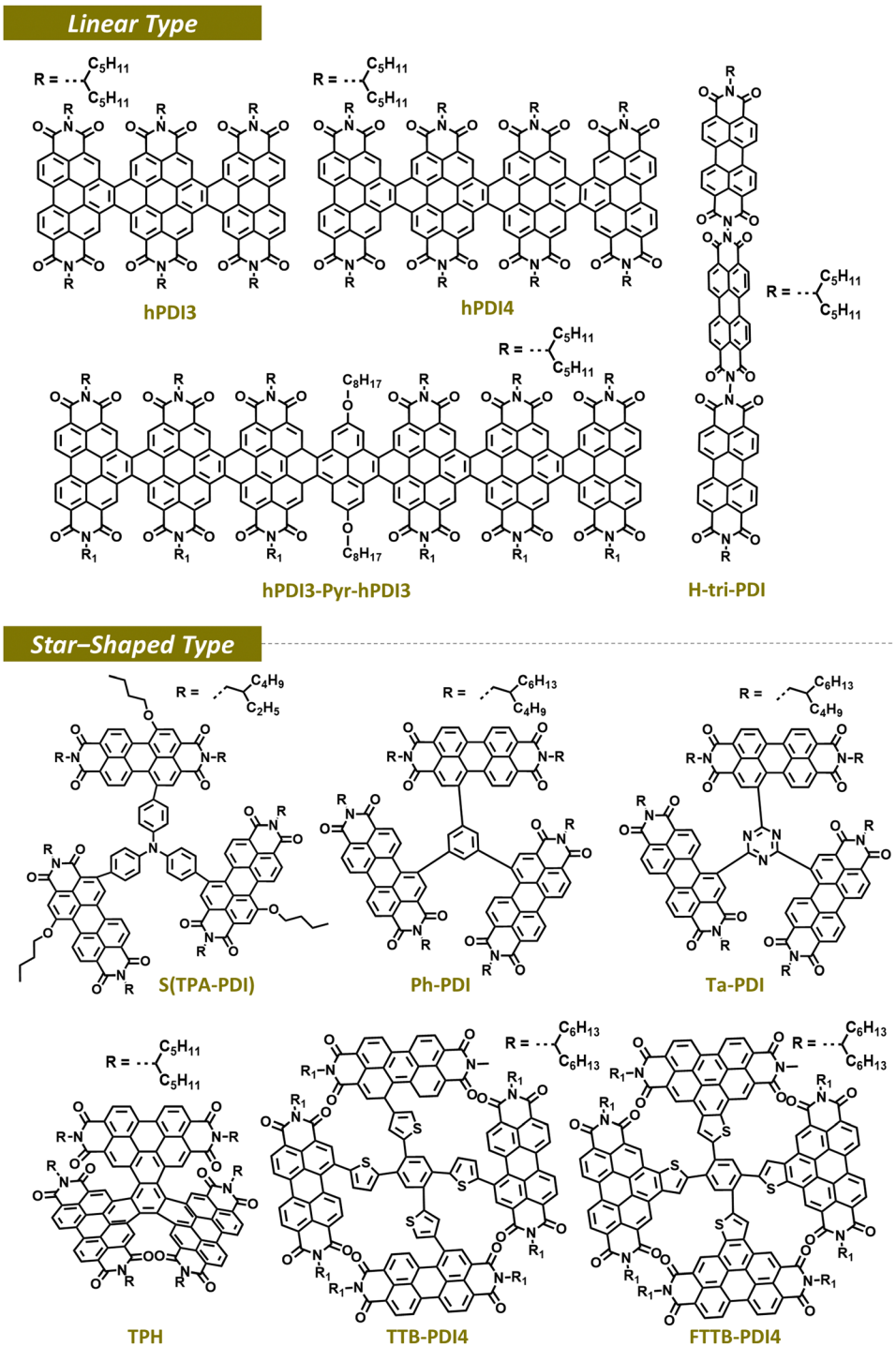

Fig. 6 Representative structures of PDI-based multimer acceptors.

exhibited twisted conformations suppressed aggregation and achieved continuous bulk-heterojunction networks in the blend with P_Ds, which are beneficial for charge generation and transport. As the π-conjugation extended from the analogous dimer to trimer (hPDI3) and tetramer (hPDI4), the absorption spectra red-shifted and the molar extinction coefficient increased, suggesting more efficient intramolecular charge transfer in hPDI4. Consequently, the PSCs based on hPDI3 and hPDI4 produced higher PCEs of 7.9 and 8.3% compared to that (6.0%) of the analogous PDI dimer.

A star-shaped PDI multimer is composed of one core block linked with multiple PDI units, thereby enabling 3-dimensional and multidirectional charge transport. In addition, because the star-shaped PDI multimers can be synthesized by simply coupling PDI monomers to a multi-armed core linker, they are much simpler to prepare compared to the linear-multimers

Table 1 Photovoltaic parameters of PSCs based on representative PDI-based trimer and tetramer acceptors

Type	Acceptor	Donor	V_{oc} (V)	J_{sc} (mA cm^{-2})	FF	PCE (%)	Ref.
Linear	hPDI3	PTB7-Th	0.81	14.5	0.67	7.9	125
	hPDI4	PTB7-Th	0.80	15.2	0.68	8.3	
	H-tri-PDI	PBDT-TS1	0.714	14.92	0.55	5.81	127
	hPDI2-Pyr-hPDI2	PTB7-Th	0.83	14.3	0.58	6.9	128
	hPDI3-Pyr-hPDI3		0.80	15.1	0.63	7.6	
	SNTP	PTB7-Th	0.77	15.22	0.60	7.17	129
	bbb-3PDI	PTB7-Th	0.764	18.13	0.51	7.12	130
Star	S(TPA-PDI)	PBDTTT-C-T	0.88	11.92	0.34	3.32	114
	TPE-PDI$_4$	PBDTT-F-TT	0.91	11.7	0.52	5.53	112
	tetra-PDI	PBDTT-F-TT	0.86	8.25	0.48	3.54	131
	Me-PDI$_4$	PBDTTT-C-T	0.77	7.83	0.45	2.73	132
	TPC-PDI$_4$	PffBT4T-2DT	0.96	9.2	0.49	4.3	133
	TPSi-PDI$_4$		0.94	8.5	0.53	4.2	
	TPGe-PDI$_4$		0.92	5.0	0.37	1.6	
	SF-PDI4	PV4T2FBT	0.90	12.02	0.54	5.98	134
	TPB	PTB7-Th	0.79	17.9	0.58	8.47	135
	B(PDI)$_3$	PTB7-Th	0.83	13.12	0.52	5.65	136
	TPH	PDBT-T1	0.968	12.01	0.70	8.28	137
	TPH-Se		1.001	12.53	0.72	9.28	
	TPPz-PDI$_4$	PffBT-T3(1,2)-2	0.987	12.5	0.56	7.1	115
	TPE-PDI$_4$		1.029	10.6	0.54	6.0	
	TPC-PDI$_4$		1.039	8.7	0.51	4.7	
	SF-iPDI4	PTB7-Th	0.82	11.36	0.50	4.68	138
	*β*TPB6-c	PTB7-Th	0.92	14.7	0.56	7.69	139
	PBI-Por	PBDB-T	0.78	14.5	0.66	7.4	140
	Ta-PDI	PTB7-Th	0.78	17.10	0.69	8.91	126
	Ph-PDI		0.85	11.91	0.55	5.15	
	P4N4	PDBT-T1	0.958	9.40	0.63	5.71	141
	TriPDI	PTB7-Th	0.85	6.13	0.38	2.19	142
	Fused-TriPDI		0.91	12.39	0.55	6.19	
	TTB-PDI4	P3TEA	1.05	12.06	0.53	7.11	39
	FTTB-PDI4		1.13	13.89	0.66	10.58	
	6T-PDI$_4$	PTB7-Th	0.82	10.69	0.47	4.12	143
	SCPDT-PDI4	PTB7-Th	0.84	14.60	0.58	7.11	144
	4PDI-ZnP	PTB7-Th	0.90	15.43	0.69	9.64	145
	p-PIB	PTB7-Th	0.82	12.32	0.59	5.95	146
	BPT-S	PDBT-T1	1.02	11.78	0.68	8.28	113
	PDI-III	PBDB-T	0.85	11.87	0.59	6.00	147
	a-FTTN-PDI4	P3TEA	1.15	12.0	0.61	8.6	148
	*o*CP-FPDI4	P3TEA	1.16	13.47	0.56	9.06	40
	SF-4PDI-O	PDBT-T1	1.014	12.44	0.71	8.90	149

requiring sequential synthetic steps. Similar to linear dimers and multimers, the molecular conformation and optoelectronic properties of star-shaped PDI multimers are significantly influenced by their linker structure. Yan group developed PDI tetramers, where four PDI units were connected to a tetrathienylbenzene core linker in a non-fused (TTB-PDI4) or fused (FTTB-PDI4) manner (Fig. 6).[39] TTB-PDI4 showed a highly distorted propeller shape, while FTTB-PDI4 possessed a double-decker structure with suppressed intramolecular twisting. And, FTTB-PDI4 showed higher absorption coefficients, and higher charge transport capabilities. These favorable properties of FTTB-PDI led to a PCE of 10.58% significantly higher than that of TTB-PDI (PCE = 7.11%). In addition, Peng group compared the PDI trimers, Ta-PDI and Ph-PDI, featuring different core linkers of 1,3,5-triazine and benzene, respectively.[126] The triazine core linker, devoid of a hydrogen atom, can eliminate potential steric hindrance with the benzene block and adjacent PDI units. As a result, in the Ph-PDI, all three PDI subunits exhibited significant twisting from the core with large dihedral angles. Conversely, in Ta-PDI, two of the three PDI subunits were aligned. Therefore, Ta-PDI had higher absorption coefficients, crystallinities, and electron mobilities. These beneficial features of the Ta-PDI molecules were successfully translated to a higher PCE of 9.15% in the Ta-PDI-based PSCs, in comparison to that (PCE = 5.57%) of Ph-PDI-based PSCs. Despite different design principles and goals, insights gained from the relationship between molecular structures, material properties, and PSC performance in PDI dimers and multimers have paved the way for the evolution of recent OSMAs based on ladder-based non-fullerene SMAs, which will be discussed in the following section.

3. Recent development of Y acceptor-based DSMA and OSMA

Ladder-type SMAs with an A–DA′D–A backbone configuration feature reinforced intrachain push–pull interactions, exhibiting markedly superior electron mobilities and light absorption abilities compared to those of traditional PDI acceptors.

Various Y-SMA derivatives have been constructed into highly efficient PSCs with a PCE above 19%.[89,92,93] However, most of these SMA-based PSCs have insufficient long-term stability due to rapid blend morphology degradation upon exposure to heat and light. This instability is associated with low T_g and high D of the SMAs, inherent to their small molecular sizes.[26,27,67] In contrast, OSMAs have higher T_gs and lower Ds compared to SMAs. Simultaneously, discrete OSMAs form strong intermolecular assemblies with high electron mobilities, differentiating them from PSMAs. As a consequence, PSCs based on Y-based OSMAs enable excellent PCEs (>18%) and outstanding long-term stability, combining the benefits of SMA- and PSMA-based PSCs.[68,71,150] In the following section, we will provide an overview of the recent advancements in Y-based OSMAs, with an emphasis on understanding the underlying design and operating principles. First, we will describe factors for the low long-term stability of SMA-based PSCs and explain how OSMAs address these performance limitations. Subsequently, we will describe a variety of recently-developed OSMAs, categorizing them based on key structural aspects, namely core-linked and end-linked configurations. Then, we will discuss how these structural features correlate with their material properties, as well as with photovoltaic performances.

3.1 Long-term device stability of PSCs

Long-term stability is a critical requirement for the successful commercialization of PSCs. Multiple factors impact this stability, such as changes in blend morphology, diffusion at the electrode interfaces, oxidation, and the formation of trap states. Among these, blend morphology degradation is a particularly important factor.[26,27,29,151] The blend morphology of the active layers in PSCs plays a critical role in influencing charge generation, transport, and collection, thereby directly affecting their PCEs. To optimize the blend morphology, various techniques (*i.e.*, incorporation of additives, thermal or solvent-vapor annealing, and physical rubbing) are employed either before or after film formation.[152–155] However, these optimal blend morphologies are not thermodynamically stable and are susceptible to degradation over time.[26–28] Accelerated degradation can occur under elevated temperatures and light exposure, triggering diffusion of both donor and acceptor molecules. This diffusion further drives phase separation between donor and acceptor components, compromising the optimized blend morphology and PCE of the PSCs.

Consequently, the long-term stability of PSCs is closely related to the diffusion kinetics of the donor and acceptor molecules within the blend film. Specifically, SMAs, which have smaller molecular sizes, exhibit higher Ds than P_D materials, making them a key cause in morphological degradation.[28,29,43,67] For instance, the diffusion coefficient at 85 °C (D_{85}) values for the majority of high-performing SMAs often exceed 10^{-18} cm^2 s^{-1}, implying that these molecules traverse more than 4 nm in a single day.[27,28,73] Considering that the optimal blend morphologies feature characteristic domain sizes of 10–30 nm, such movement represents a significant change.

The diffusion kinetics of SMAs are also closely related to their T_g or T_{cc} in the film. These parameters indicate the temperature at which imperfect SMA crystals that form during solution processing of films become mobile and start to reorganize. In a detailed study on the long-term stability of PSCs, the Ade group examined the relationship between the T_g and D of various SMA molecules, exploring more than ten different blend systems with five distinct SMAs and four unique P_D pairs.[27] They found that the diffusion kinetics of SMAs within the blend film follows the Arrhenius equation, revealing a direct correlation between T_g and D of $D = A \times \exp(B \times (-T_g))$, where A and B are constants that are influenced by the donor types. As a result, the morphological stability of the active layers is largely affected by (1) diffusion kinetics of the SMAs and (2) thermodynamic interaction between the SMAs and P_Ds. Recently, the Lipomi group introduced a simple and straightforward method to estimate the T_g values of SMAs in their films by monitoring changes in UV-Vis absorption spectra under different annealing temperatures.[156] This is a simpler approach compared to time-of-flight secondary ion mass spectrometry experiments to determine the D values of the SMAs at various temperatures and annealing durations.[27,28,156] Consequently, T_g has emerged as a critical parameter for predicting both the diffusion kinetics of SMAs and the long-term stability of PSCs.

Recent studies have demonstrated that OSMAs (*i.e.*, dimer, trimer, and tetramer) possess significantly higher T_g values (>130 °C) compared to SMAs (<100 °C).[28,42,67,73,151,157] This distinction yields markedly prolonged lifetime for OSMA-based PSCs. The increased OSMA chain lengths effectively restrict thermal diffusion, thereby maintaining the blend morphology. Furthermore, due to their discrete and appropriate molecular sizes, these OSMAs retain sufficient crystallinity and electron mobility, resulting in high J_{sc} and FF values for their PSCs. An additional benefit for the OSMAs is the incorporation of electron-donating spacers connecting SMA units. This design successfully elevates their LUMO energy levels compared to SMAs, leading to a V_{oc} of over 0.9 V for PSCs. Consequently, PSCs featuring OSMAs demonstrate not only excellent PCE above 18% but also significantly improved long-term stability.

The photovoltaic performance and device stability of recently developed OSMA-based PSCs are summarized in Table 2. In addition, their PCE and stability compared to traditional SMA-based PSCs or PSMA-based all-PSCs are illustrated and compared in Fig. 7. The stability of each PSC is quantified using a $t_{80\%}$ lifetime metric, which signifies the time for the PCE to reach 80% of its initial value under heat or light exposure. As shown in Fig. 7, SMA-based PSCs display a high PCE but low stability, whereas PSMA-based all-PSCs exhibit high stability but a relatively low PCE. In contrast, PSCs based on OSMAs with the same backbone show high PCE (>18%) and excellent stability ($t_{80\%}$ lifetime >1000 h). Considering the nascent stage of research on these OSMAs, we anticipate that the development of advanced OSMAs, guided by comprehensive knowledge of their operating mechanisms and design principles, will lead to commercially viable high-performance PSCs with sufficient long-term stability.

Table 2 Photovoltaic performances and device stabilities of reported DSMA- and OSMA-PSCs

Acceptor	Material type	V_{oc} (V)	PCE_{max} (%)	Stability condition	Device stability[a]	Ref.
BTICγ-EH	SMA	0.95	7.24	1 sun	$t_{80\%}$ = 260 h	70
dBTICγ-EH	OSMA	0.92	14.48	1 sun	$t_{80\%}$ = 1020 h	
dBTICγ-BO	OSMA	0.91	13.42	1 sun	$t_{80\%}$ = 840 h	
tBTICγ-BO	OSMA	0.90	13.16	1 sun	$t_{80\%}$ = 840 h	
pBTICγ-OD	PSMA	0.91	12.15	1 sun	$t_{80\%}$ = 600 h	
Monomer	SMA	0.925	16.54	1 sun	$t_{80\%}$ = 62 h	71
2BTP-2F-T	OSMA	0.911	18.19	1 sun	$t_{80\%}$ = 443 h	
PYF-T-o	PSMA	0.889	15.86	1 sun	$t_{80\%}$ = 185 h	
OY1	SMA	0.827	14.20	1 sun	$t_{80\%}$ = 1535 h	67
OY2	OSMA	0.837	14.82	—	—	
OY3	OSMA	0.839	15.05	1 sun	$t_{80\%}$ = 25 000 h	
OY4	OSMA	0.814	14.97	—	—	
POY	PSMA	0.833	14.12	1 sun	$t_{80\%}$ = 2385 h	
Y6	SMA	0.84	16.93	1 sun	$t_{60\%}$ = 120 h	158
DY1	OSMA	0.87	16.46	—	—	
DY2	OSMA	0.87	17.85	1 sun	$t_{83\%}$ = 700 h	
DY3	OSMA	0.87	17.33	—	—	
DYT	OSMA	0.94	17.30	1 sun	$t_{80\%}$ = 2493 h	157
DYV	OSMA	0.93	18.60	1 sun	$t_{80\%}$ = 4005 h	
DYTVT	OSMA	0.95	17.68	1 sun	$t_{80\%}$ = 5419 h	
MYBO	SMA	0.877	17.12	1 sun	$t_{80\%}$ = 36 h	42
DYBO	OSMA	0.968	18.08	1 sun	$t_{80\%}$ = 6085 h	
CH8-0	OSMA	0.936	15.26	65 °C	$t_{78\%}$ = 360 h	159
CH8-1	OSMA	0.923	17.05	1 sun	$t_{85\%}$ = 200 h	
CH8-2	OSMA	0.928	16.84	65 °C	$t_{85\%}$ = 360 h	
Y6	SMA	0.86	17.41	1 sun	$t_{80\%}$ = 170 h	74
Y6 : dT9TBO (1.1 : 0.1)	SMA + OSMA	0.88	18.41	1 sun	$t_{80\%}$ = 500 h	
PZC24	PSMA	0.946	16.82	1 sun + 65 °C	$t_{80\%}$ = 320 h	150
PZC24 : CH-D1 (1 : 0.3)	PSMA + OSMA	0.949	17.40	1 sun + 65 °C	$t_{80\%}$ = 350 h	
ECOD	SMA	0.843	16.40	N_2	$t_{80\%}$ = 800 h	160
EV-i	OSMA	0.897	18.27	N_2	$t_{90\%}$ = 800 h	
EV-o	OSMA	0.957	2.50	—	—	
MYT	SMA	0.917	16.44	1 sun	$t_{80\%}$ = 35 h	73
DYT	OSMA	0.942	17.29	1 sun	$t_{80\%}$ = 2551 h	
TYT	OSMA	0.964	18.15	1 sun	$t_{80\%}$ = 8454 h	
BTP-eC9	SMA	0.855	17.8	120 °C	$t_{63\%}$ = 200 h	161
BTP-eC9 : DT19 (1 : 0.2)	SMA + OSMA	0.866	18.2	120 °C	$t_{90\%}$ = 200 h	
DIBP3F-Se	OSMA	0.917	18.09	85 °C	$t_{80\%}$ = 22 days	162
DIBP3F-S	OSMA	0.901	16.11	85 °C	$t_{80\%}$ = 13 days	
DYA-I	OSMA	0.938	18.83	1 sun	$t_{80\%}$ = 5380 h	72
DYA-IO	OSMA	0.948	17.54	1 sun	$t_{80\%}$ = 4255 h	
DYA-O	OSMA	0.961	16.45	1 sun	$t_{80\%}$ = 3375 h	
Y6-OD	SMA	0.848	17.46	1 sun	$t_{80\%}$ = 1523 h	151
Tri-Y6-OD	OSMA	0.916	18.03	1 sun	$t_{80\%}$ < 50 h	
CH8-3	OSMA	0.915	17.22	1 sun	$t_{80\%}$ ~ 250 h	163
CH8-4	OSMA	0.894	17.58	1 sun	$t_{80\%}$ ~ 250 h	
CH8-5	OSMA	0.902	16.79	1 sun	$t_{80\%}$ ~ 250 h	
DYV	OSMA	0.910	18.01	1 sun	$t_{80\%}$ ~ 700 h	164
DYC10	OSMA	0.947	14.48	1 sun	$t_{77\%}$ ~ 700 h	
P2EH	OSMA	0.905	17.09	85 °C	$t_{85\%}$ ~ 1100 h	65
P2EH:BTP-eC9	SMA + OSMA	0.871	19.09	85 °C	$t_{85\%}$ ~ 1100 h	
Dimer-QX	OSMA	0.933	14.59	80 °C	$t_{80\%}$ ~ 11 261 h	165

Table 2 (*continued*)

Acceptor	Material type	V_{oc} (V)	PCE_{max} (%)	Stability condition	Device stability[a]	Ref.
Dimer-2CF	OSMA	0.900	19.02	80 °C	$t_{80\%}$ ~ 11 983 h	
G-Dimer	OSMA	0.904	17.41	80 °C	$t_{90\%}$ ~ 4500 h	166
G-Trimer	OSMA	0.896	19.01	80 °C	$t_{80\%}$ ~ 4500 h	
PSMA	PSMA	0.892	15.86	80 °C	$t_{80\%}$ ~ 200 h	
TDY-α	OSMA	0.864	18.1	1 sun	$t_{80\%}$ ~ 34 747 h	167
TDY-β	OSMA	0.849	17.0	1 sun	$t_{80\%}$ ~ 31 000 h	
dBTIC-δV-BO	OSMA	0.96	13.15	1 sun	$t_{80\%}$ ~ 750 h	168
dBTIC-γV-BO	OSMA	0.91	17.14	1 sun	$t_{80\%}$ ~ 2150 h	
dBTIC-γV-OD-2Cl	OSMA	0.87	16.04	1 sun	$t_{80\%}$ ~ 1100 h	
Tet-0	OSMA	0.914	16.63	1 sun	$t_{80\%}$ ~ 216 h	169
Tet-1	OSMA	0.919	17.32	1 sun	$t_{80\%}$ ~ 288 h	
Tet-3	OSMA	0.921	16.92	1 sun	$t_{80\%}$ ~ 264 h	
DYT	OSMA	0.948	17.20	1 sun	$t_{80\%}$ ~ 2157 h	170
TYT-S	OSMA	0.964	18.61	1 sun	$t_{80\%}$ ~ 2604 h	
DYSe-I	OSMA	0.94	16.8	100 °C	$t_{80\%}$ ~ 514 h	171
DYSe-O	OSMA	0.95	14.0	100 °C	$t_{80\%}$ ~ 115 h	
N3	SMA	0.83	17.56	1 sun	$t_{80\%}$ ~ 200 h	172
DP-BTP	OSMA	0.96	15.08	1 sun	—	
N3:DP-BTP	SMA + OSMA	0.87	19.07	1 sun	$t_{80\%}$ ~ 4983 h	
2Y-Wing	OSMA	0.850	17.73	80 °C	$t_{90\%}$ ~ 200 h	173
2Y-Core	OSMA	0.864	5.63	80 °C	$t_{67\%}$ ~ 200 h	
2Y-End	OSMA	0.948	14.46	80 °C	$t_{32\%}$ ~ 200 h	

[a] $t_{x\%}$ indicates the time taken for the PSC performance to degrade to x% of the initial PCE.

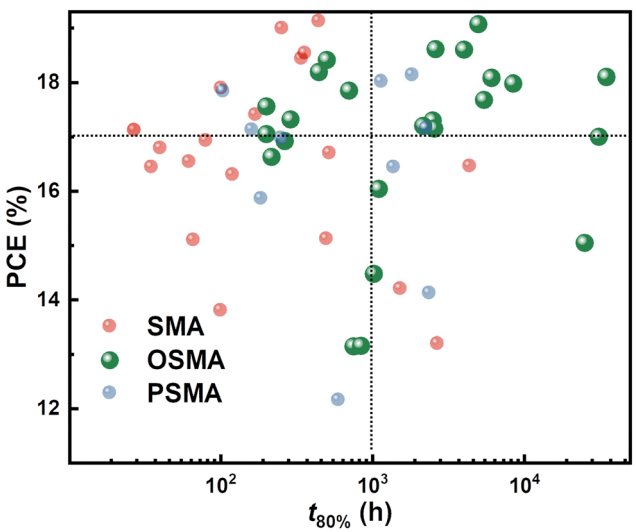

Fig. 7 PCE and $t_{80\%}$ lifetime under 1 sun illumination of the PSCs based on different acceptor material types.

3.2 Development of Y-based DSMAs

As the Y-based SMAs are among the most efficient ladder-based non-fullerene SMAs, most recent OSMAs are based on these Y-based SMAs.[68,109] In subsequent sections, we will focus on the development and characteristics of OSMAs derived from Y-based SMAs. The molecular design of these OSMAs is categorized into three main components: (1) Y-SMA core units, (2) the length and structure of side chains, and (3) the position and structure of linkers (Fig. 8). The design principles for the core units and side chains of the OSMAs are consistent with their monomeric SMAs counterparts. However, the linker position and structure are distinct for the design of OSMAs. In this respect, recent studies have mainly examined the optimal linking positions within the SMA units and linker structure. Here, we discuss how each design parameter impacts the material properties and PSC performances of OSMAs.

The Y-based SMAs, characterized by a DA′D core structure with IC units capping each end, incorporate four side chains—two attached to the inner pyrrole rings and two to the outer thiophene rings. This structure promotes high conformational rigidity, minimizing energy loss while enhancing light absorption and charge transport capacity. Particularly, Y-based SMAs can form 2D- or 3D-packing structures through two distinct packing interactions: π–π stacking between the end groups and face-to-face π-core interaction within the core moieties. This dual interaction can facilitate the development of efficient charge transport channels. The structural advantages of Y-based SMAs have facilitated PCEs surpassing 18%, and additional structural modifications hold the potential to optimize their material properties further.

The core structure significantly influences the performance of Y-SMAs, which can be categorized based on the electron-withdrawing units into benzotriazole (BTz)-, benzothiadiazole

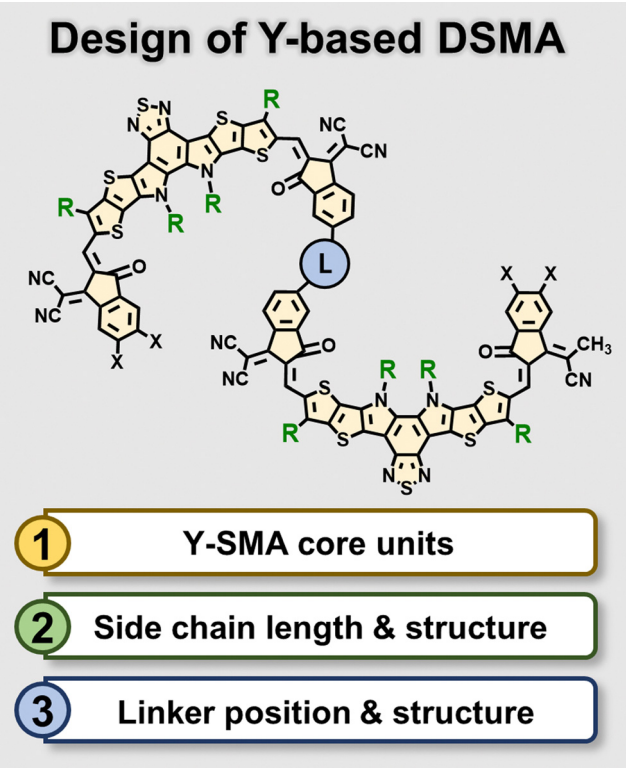

Fig. 8 General design considerations for Y-based DSMAs.

(BT)-, and quinoxaline (Qx)-based cores. The BTz core-based Y-SMAs (*i.e.*, Y1 and Y2) were first developed by the Yang group, exhibiting PCEs above 13%.[174] The SMAs based on the BT cores (*i.e.*, Y6, Y7, and BTP-eC9) were subsequently developed by the Zou group and the Hou group by replacing the nitrogen atom of BTz with sulfur.[20,92,175,176] As the BT units have stronger electron-withdrawing properties and an enhanced push–pull effect with adjacent electron-donating units compared to BTz, BT-based SMAs exhibited reinforced light absorption ability and higher electron mobility. As a result, PSCs from BT-based SMAs achieved PCEs above 18%.[14,25,92] Most recently, Qx-based SMAs (*i.e.*, Qx1 and Qx2) have been reported.[177–179] The upshifted LUMO energy levels of Qx-based SMAs afford PSCs with higher V_{oc}s than those of BT- and BTz-based SMAs.[94,163,179] In addition, the quinoid resonance effect of Qx groups reduces the reorganization energy and enhances the charge transport properties of the resulting SMAs,[150,179] contributing to a higher J_{sc} of the PSCs. As a result, Qx-based SMAs have demonstrated PSCs with comparable or higher PCEs (>18%) than BT-based SMAs.[94,179] Overall, Y-based SMAs with PCEs greater than 18% are predominantly composed of BT- or Qx-core units. The main structural difference between BT- and Qx-based core units is that the two unpaired sites of Qx units enable additional functionalization, whereas BT cores lack any functional sites. This allows for distinctive chemical modifications to the Qx cores, such as conjugation extension, side chain inclusion, and halogenation.[179] Furthermore, as it will be discussed in the next section, Qx-based SMAs can be dimerized *via* a direct core linking to yield unique dimer acceptors with core-head connected structures.

Side chains are another critical component of SMAs. Although side chains in SMAs are primarily designed to provide sufficient solubilities for their solution processing and tune their aggregation structures, the structure and length of the side chains also significantly impact the optoelectronic and crystalline properties of SMAs.[24,180,181] For Y-based SMAs, the side chains can be categorized based on their position relative to the electron-withdrawing core units: those positioned above are termed outer side chains, while those below are referred to as inner side chains. Branched alkyl side chains, such as 2-ethylhexyl or 2-butyloctyl, are typically used as the inner side chains of Y-SMAs to ensure adequate solubility. The outer alkyl chains can either be linear (like nonyl or undecyl) or branched types (*e.g.*, 2-butyloctyl). It has been reported that even minor variations in the length or structure of these side chains have a strong influence on the crystalline structure of the SMAs and the PCE of their resulting PSCs.[24,92,180] For instance, the Hou group developed three SMAs with varying lengths of linear-type outer side chains (BTP-eC7, BTP-eC9, and BTP-eC11).[92] Among them, BTP-eC9, which had medium side chains, achieved PSCs with the highest PCE of 17.8%. This was attributed to the ideal solubility and packing structure of BTP-eC9 enabling well-mixed blend morphology and fast charge transport. Furthermore, the Sun group demonstrated that substituting the outer Y-SMAs side chains from a linear (undecyl) to branched (2-butyloctyl) allowed for a more compact and three-dimensional packing structure.[24] Consequently, the SMA with branched outer side chains (L8-BO) exhibited a higher PCE of 18.32%, compared to the linear SMA analogue (Y6, PCE = 16.61%). Although the primary design rules for the side chains of OSMAs are similar to SMAs, OSMAs often require longer side chains to achieve sufficient solubility due to their larger molecular sizes. For example, the inner side chains of reported Y-based OSMAs (*i.e.*, 2-hexyldecyl or 2-octyldodecyl) are often much longer than those of monomer SMAs (*i.e.*, 2-ethylhexyl or 2-butyloctyl).

The position and structure of the linker connecting Y-SMA units are the most important parameters that should be carefully considered in the design of OSMAs. Variation in the linker position can lead to completely different OSMA molecular conformations. Two primary sites for the linker have been identified: (1) functionalization sites on the core units (*i.e.*, core-head or inner side chain), or (2) functionalization sites on the terminal IC units. Therefore, the linker positions of Y-based OSMAs can be categorized into core-linked and end-linked structures. Given that a single Y-SMA consists of one core unit and two IC end groups, the core-linking approach predominantly results in DSMA structures rather than multimers. Conversely, end-linked SMAs enable the sequential connection of multiple SMA units, resulting in the OSMAs with different chain lengths including di-, tri-, tetra-, and pentamers. For core-linked DSMAs, dimerization can take place *via* the core head or inner side chains. In the case of BT-based SMA units, which lack a functionalization site at the core head, dimerization is limited by linking through inner side chains. In contrast, for

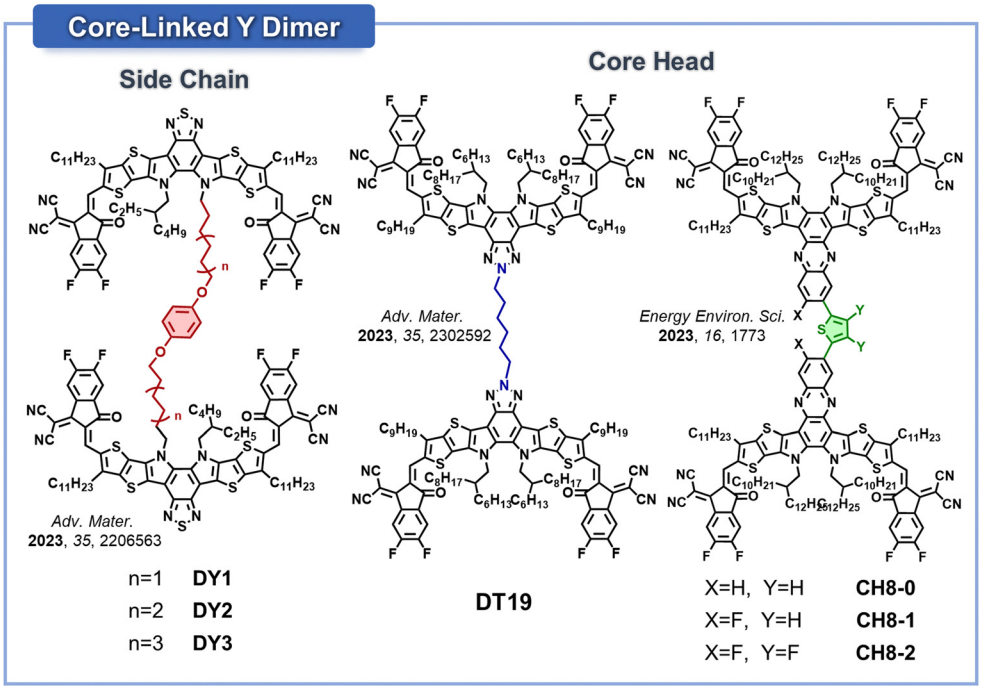

Fig. 9 Y-Based dimer acceptors bridged *via* Y-core structure.

the cases of BTz- or Qx-based SMAs, the dimerization can be achieved through both the core head and inner side chains.

Representative examples of core-linked DSMAs are illustrated in Fig. 9. The first core-linked DSMAs were developed by the Li group.[158] They used a 1,4-dialkoxyphenyl-bridged flexible spacer to dimerize BT-based Y-SMAs by linking their inner side chains. Various alkyl chain length spacers next to the phenyl groups (*e.g.*, hexyl, octyl, and decyl chains) were employed to yield three distinct DSMAs of DY1, DY2, and DY3, respectively. Among these, DY2, with a medium-length alkyl spacer, displayed PSCs with the highest PCE of 17.85%. This superior performance was mainly attributed to its strong packing structures and optimal blend morphology. Later, the Min group developed another core-linked DSMA (DT19) constructed from BTz-based Y-SMA units.[161] They connected two SMAs utilizing a hexyl linker at the core head positions of the BTz units. This DT19 DSMA was introduced as a third component in different P_D:SMA blend systems. The addition of the DSMAs improved blend morphology and reduced the diffusion of the host electron acceptors, which subsequently increased the PCE and stability of the PSCs. The PSCs based on the PM1:BTP-eC9:DT19 ternary blend displayed a high PCE of 18.2% with improved thermal stability compared to those of the PM1:BTP-eC9 binary system, which showed a PCE of 17.8%.

The Chen group developed core-linked DSMAs by utilizing Qx-based SMA units (Fig. 9 and 10).[159] These SMA units were connected by thiophene linkers, strategically positioned at the core-head locations of the Qx-based SMAs. What sets this molecular design apart from the previously mentioned core-linked DSMAs is the continuous linker conjugation, offering enhanced push–pull effects throughout their molecular backbones. To tune the three-dimensional conformation of the DSMAs, fluorine atoms were sequentially introduced to the Qx cores and thiophene linkers. This modification brought about three distinct DSMAs: CH8-0, CH8-1, and CH8-2 (Fig. 9).[159] They observed that increased fluorine atoms improved the planarity of the DSMA backbones, as evidenced by decreased dihedral angles between the two SMA planes from 59 to 19°. (Fig. 10). The increased crystallinity promoted the formation of larger nanofibrils of the DSMAs as shown in atomic force microscopy (AFM) images, which played a crucial role in optimizing electron transport in the blend films. Consequently, CH8-1 and CH8-2, exhibited PCEs of 17.05 and 16.84%, respectively, outperformed the non-fluorinated DSMA, CH8-0, which posted a PCE of 15.26%.

In their subsequent study, the Chen group developed new core-linked DSMAs (CH8-3, CH8-4, and CH8-5) based on the same Qx-based SMA backbones, but varied the halogen atoms in the core units and IC end-groups.[163] Specifically, CH8-4, with fluorine atoms in the core unit and chlorine atoms in the IC end-groups, showed relatively small dihedral angles between its two SMA planes (36°) compared to those in CH8-5 and CH8-6 (>80°). This feature endowed CH8-4 with superior crystallinity and electron mobility among the DSMA series, leading to the highest PCE of 17.6% in the PSCs. Additionally, all the three new DSMAs demonstrated similar high photostability, with $t_{80\%}$ lifetimes of ~250 h under 1 sun illumination. CH8-4 was successfully used to produce a PSC module with an active area of 2.88 cm^2 and a PCE over 13%.

For end-linked oligomer acceptors, the SMA units are connected *via* their terminal IC units by conjugated linkers. This oligomerization typically employs a Stille condensation, which

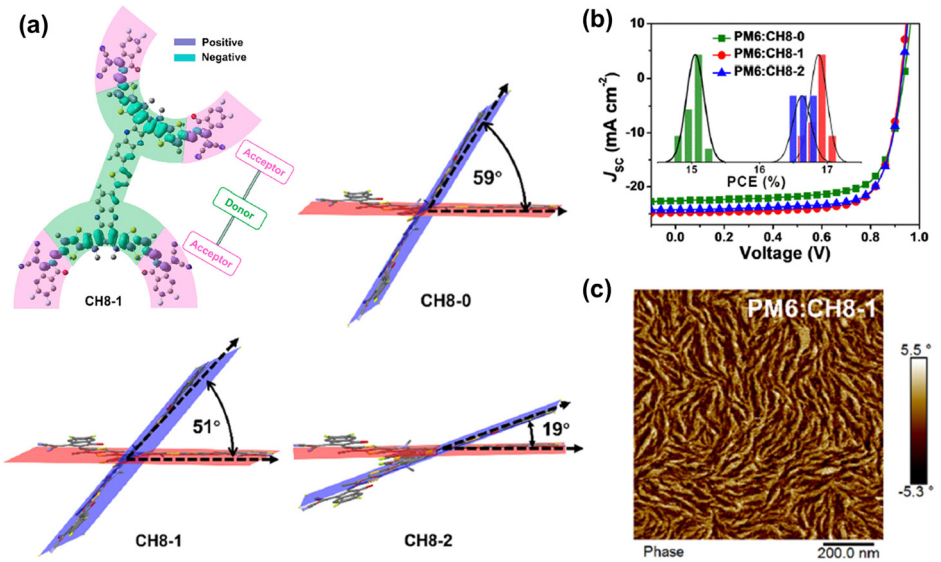

Fig. 10 (a) Theoretical density distribution of CH8-1 and ground-state geometries of CH8-*x* dimers calculated by the DFT method. (b) *J*–*V* curves and PCE distributions of PM6:CH8-*x* PSCs. (c) AFM phase image of the PM6:CH8-1 blend film. Reproduced from ref. 159 with permission from the Royal Society of Chemistry, copyright 2024.

combines Br-terminated SMA cores with Sn-terminated linkers. This process is similar to the polymerization of PSMAs. The synthetic details of end-linked oligomer acceptors will be discussed in the next section. Inspired by the synthetic strategies for PSMAs, a large variety of DSMAs and multimers have been developed using the end-linking approach compared to core-linked DSMAs. The molecular structures of these end-linked DSMAs are depicted in Fig. 11.

He group has developed an end-linked DSMA, named dBTICγ-EH, by directly coupling monobrominated Y-SMA units *via* Stille-Kelly condensation, without employing an additional linker.[70] They demonstrated that the dBTICγ-EH DSMA-based PSCs have a higher PCE (16.1%) than monomeric SMA-based PSCs (BTIC-EH, PCE = 12.1%) and PSMA (pBTICγ-BO, PCE = 12.6%). Following this, the Wei group reported another dimerized acceptor, 2BTP-2F-T, consisting of Y-series SMAs linked by a thiophene unit.[71] When paired with a PM6 P_D, the 2BTP-2F-T acceptor resulted in highly efficient PSCs with a PCE of 18.2%. They also observed that thiophene linkers effectively enhanced the backbone planarity of the DSMAs by reducing the dihedral angles between the Y-core units from 35 to 20°.

Kim group developed a new DSMA (DYBO), which incorporated BT-based Y-SMAs and benzodithiophene (BDT) linkers.[42] We found that incorporation of the electron-donating BDT linkers effectively upshifted the LUMO energy level of DYBO (to −3.96 eV) compared to the monomer SMA (MYBO, LUMO = −4.04 eV), while the maximum absorption wavelength in film (λ_{max}) of DYBO (805 nm) was slightly blue-shifted compared to that of MYBO (λ_{max} = 816 nm). Moreover, BDT linkers were shown to effectively reduce torsion between Y-SMA units, resulting in a small dihedral angle of 8.5°, compared to the 19.5° angle with thiophene linkers. This ensured a more planar backbone conducive to compact and strong molecular packing. Consequently, DYBO had an electron mobility (5.1×10^{-4} cm^2 V^{-1} s^{-1}) comparable to that of the MYBO (5.9×10^{-4} cm^2 V^{-1} s^{-1}). In particular, DYBO exhibited significantly higher T_g (179 °C) and lower D_{85} values (4.3×10^{-23} cm^2 s^{-1}) compared to MYBO (T_g = 80 °C and $D_{85} = 1.2 \times 10^{-16}$ cm^2 s^{-1}). As a result, DYBO-based PSCs demonstrated higher V_{oc} (0.968 V), PCE (18.08%), and photostability ($t_{80\%}$ lifetime = 6085 h under 1 sun illumination) compared to the MYBO-based PSCs (V_{oc} = 0.877 V, PCE = 17.12%, and $t_{80\%}$ lifetime = 36 h). Additionally, it was noted that the enhanced molecular compatibility of DYBO with PM6 P_D, in comparison to MYBO with PM6, also contributed to superior device stability of DYBO-OSCs. This is because DYBO and PM6 share the same BDT units, which was helpful in preventing excessive phase separation. This highlights the necessity of considering molecular interaction parameters in the DSMAs design, in addition to their diffusion kinetics.

In a following study, our group further elucidated the significance of selecting appropriate linkers for optimizing DSMAs properties (Fig. 12).[157] Three distinct DSMAs were synthesized using different linkers including thiophene (DYT), vinylene (DYV), and thiophene-vinylene-thiophene (DYTVT). Intriguingly, a correlation between the linker structure and the overall planarity of the DSMA backbones was observed. Specifically, the dihedral angles between SMA units showed a decreasing trend, with angles of 18.7° for DYT, 15.8° for DYV, and 14.8° for DYTVT. The shift in planarity resulted in enhanced aggregation, crystallinity and electron mobilities of the DSMAs. Regarding photovoltaic performances, PSCs based on DYV DSMAs exhibited the highest PCE of 18.60% in the series. This result is attributed to the high electron mobility of DYV DSMAs and optimal phase separation of DYV-based blend films. Though DYTVT had the highest electron mobility, its strong crystallization drove excessively phase separated blend

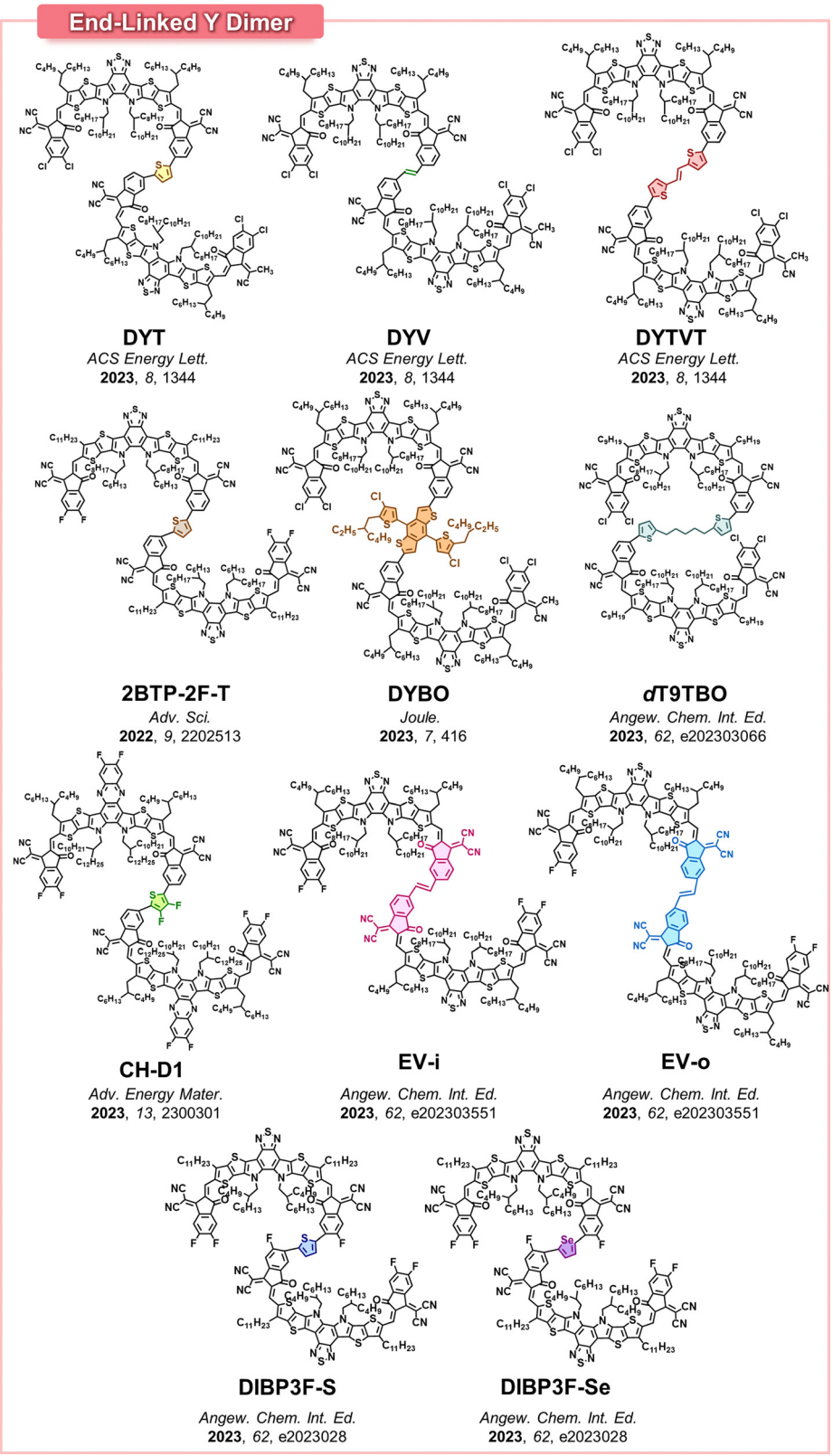

Fig. 11 Y-Based DSMAs bridged *via* end groups of the Y monomers.

morphologies, resulting in lower charge generation and PCE values in their PSCs. In addition to PCE, the DSMA backbone planarity significantly affected their T_gs and long-term stability of the PSCs. Specifically, the T_g of the DSMAs and the $t_{80\%}$ lifetime of their resultant PSCs were gradually enhanced with increasing planarity of the linkers: DYT (T_g = 123 °C and $t_{80\%}$

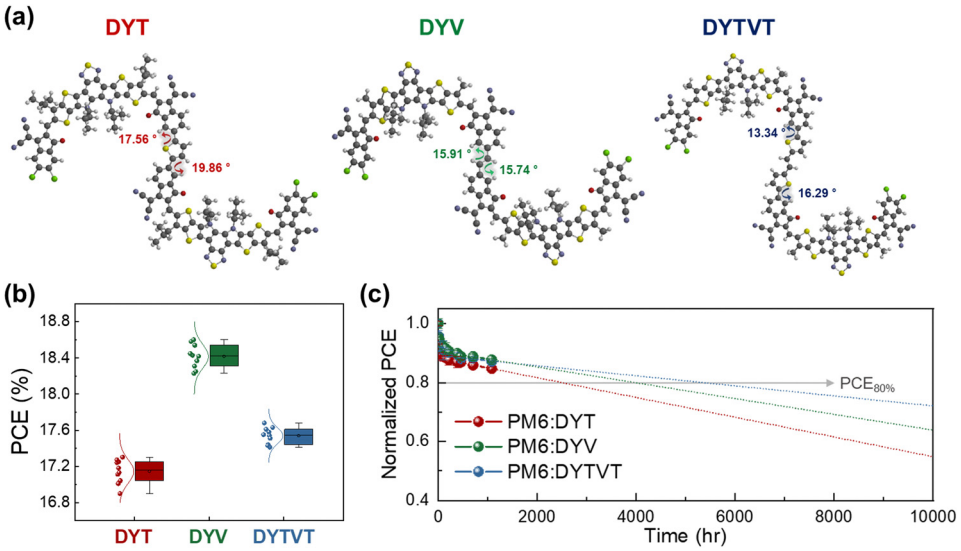

Fig. 12 (a) Optimized molecular conformations and dihedral angles of DYT, DYV, and DYTVT. (b) PCE and (c) photo-stability of Y dimer-based PSCs. Reproduced from ref. 157 with permission from the American Chemical Society, copyright 2024.

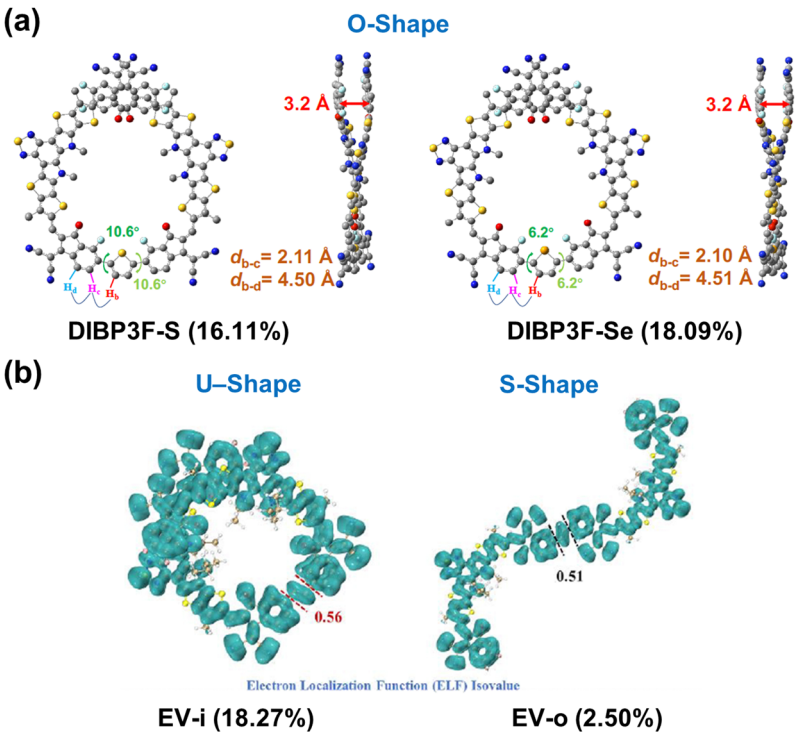

Fig. 13 Various molecular conformations of DSMAs achieved by modification of linker structure and position; (a) DIBP3F-S and DIBP3F-Se and (b) EV-i and EV-o. Reproduced from ref. 160 and 162 with permission from the John Wiley & Sons, Inc., copyright 2024.

lifetime = 2493 h) < DYV (T_g = 134 °C and $t_{80\%}$ lifetime = 4005 h) < DYTVT (T_g = 140 °C and $t_{80\%}$ lifetime = 5419 h).

In another study, the Wang group developed end-linked DSMAs with thiophene and selenophene linkers (DIBP3F-S and DIBP3F-Se, respectively) and highlighted the crucial role of conformational locking between IC units and linkers in DSMAs (Fig. 13a).[162] They strategically positioned a fluorine atom at the third position of the IC units, adjacent to the linkers. This allowed the fluorine atoms to form strong non-covalent interactions with the hydrogen atoms on the linker. Therefore, both DIBP3F-S and DIBP3F-Se DSMAs showed highly planar backbones. Interestingly, it was observed that strong F···H interactions between IC units and linkers resulted in an O-shaped molecular DSMA conformation. Both DIBP3F-S and

DIBP3F-Se displayed high crystallinity and SCLC electron mobility of 7.77 × 10^{-4} $cm^2 V^{-1} s^{-1}$ and 8.95 × 10^{-4} $cm^2 V^{-1} s^{-1}$, respectively. Among the two DSMAs, DIBP3F-Se outperformed DIBP3F-S in terms of electron mobility, leading to a higher PCE in the corresponding PSCs (18.1 *vs.* 16.1%).

Beyond the architectural modification, the regiospecific linker placement also significantly contributes to achieving a high backbone planarity in end-linked DSMAs. The widely used terminal unit, brominated 1,1-dicyanomethylene-3-indanone (IC-Br), is categorized into two types of regioisomers, namely IC-Br-In and IC-Br-Out, depending on whether the bromine groups are attached to the carbonyl or dicyanide side of the IC units, respectively.[59,60,182] This leads to two distinct regiospecific linker positions during condensation coupling, which has a direct impact on the overall molecular conformation, crystallinity, and electron mobility of the DSMAs. The impact of regiospecific linker incorporation has been demonstrated in various PSMAs.[16,59,60,98,102,183] For instance, the Yang group showed that the PSMA using IC-Br-In (PY-IT) exhibited enhanced aggregation and crystalline properties compared to IC-Br-Out (PY-OT) based materials.[98] Consequently, all-PSCs based on PY-IT achieved a higher PCE of 15.05% compared to those based on PY-OT, which had a PCE of 10.04%.

Li group was the first to emphasize the significance of regioselective linker incorporation in DSMAs.[160] They engineered two regiospecific end-linked DSMAs with vinylene linkers (EV-i and EV-o) using IC-Br-In and IC-Br-Out units for the dimerization of Y-SMAs, respectively (Fig. 13b). They discovered that EV-i and EV-o exhibited very different molecular conformations. EV-i adopted a U-shaped conformation, while EV-o possessed an S-shape in their optimized states. The U-shaped conformation of EV-i was more conducive to compact molecular packing and superior intermixing with the P_D compared to the S-shaped EV-o. As a result, blend films based on EV-i exhibited an order of magnitude higher electron mobility (2.07 × 10^{-4} $cm^2 V^{-1} s^{-1}$) and a much smoother blend morphology (average surface roughness in an AFM height image= 1.3 nm) than EV-o blend films (electron mobility = 2.85 × 10^{-5} $cm^2 V^{-1} s^{-1}$, average surface roughness = 14.6 nm). Consequently, PSCs based on EV-i blends showed a significantly higher PCE of 18.27%, compared to 2.50% for the EV-o-based PSCs. The particularly low PCE of the EV-o-based PSCs was attributed to inefficient charge generation and transport, stemming from excessively large domain sizes and low electron mobility.

Around the same time, our group also developed a series of regioisomerically pure DSMAs and demonstrated the significance of regiospecific linker placement in DSMAs for optimizing both PCE and long-term stability of the resulting PSCs.[72] We have synthesized a series of regioisomeric DSMAs featuring acetylene linkers (DYA-I, DYA-IO, and DYA-O). Specifically, DYA-I was synthesized by dimerizing SMA units with IC-Br-In, while DYA-O used IC-Br-Out. Meanwhile, DYA-IO was synthesized by employing both regioisomers on either side. It was observed that the DSMA backbone planarity increased sequentially in the order of DYA-O, DYA-IO, and DYA-I, as evidenced by decreasing dihedral angles between the SMA constituent units in the optimized states: DYA-O (18.8°) > DYA-IO (15.9°) > DYA-I (12.2°). As a result, the crystallinity, electron mobility, and T_g of the DSMAs increased in the order of DYA-O (melting temperature (T_m) = 255 °C, electron mobility = 1.1 × 10^{-4} cm^2 V^{-1} s^{-1}, and T_g = 131 °C), DYA-IO (T_m = 264 °C, electron mobility = 3.4 × 10^{-4} cm^2 V^{-1} s^{-1}, and T_g = 137 °C), and DYA-I (T_m = 268 °C, electron mobility = 4.7 × 10^{-4} $cm^2 V^{-1} s^{-1}$, and T_g = 142 °C). This, in turn, enhanced the PCE and device stability of the resulting PSCs in the same order; DYA-O (PCE = 16.45% and $t_{80\%}$ lifetime = 3377 h) < DYA-IO (PCE = 17.54% and $t_{80\%}$ lifetime = 4255 h) < DYA-I (PCE = 18.83% and $t_{80\%}$ lifetime = 5380 h).

Recently, DSMAs with different types of molecular structures other than end-linked and core-linked structures have been developed. Li group synthesized a center-fused type DSMA, DP-BTP, containing pyrene at the central core *via* the dehydration process of diamine and 4,5,9,10-pyrenetetraone (Fig. 14a).[172] The fused backbone structure of DP-BTP DSMA resulted in negligible torsion between the two Y-core units, which was advantageous for obtaining excellent light absorption and charge transport capabilities. When combined with D18 P_D, D18:DP-BTP-based PSCs exhibited a high PCE of 15.08%. When DP-BTP was used as the third component in a high-performance SMA (N3)-based system, the D18:N3:DP-BTP ternary PSCs achieved a higher PCE of 19.07%. In addition, D18:N3:DP-BTP-based PSCs demonstrated considerably greater photostability ($t_{80\%}$ lifetime = 4963 h) than the D18:N3-based devices ($t_{80\%}$ lifetime = 200 h), owing to the higher T_g (126 °C) of DP-BTP compared to the N3 SMA (T_g = 88 °C).

More recently, Fan group developed a wing-site connected DSMA, named 2Y-wing, by connecting two Y-core units *via* the outer side-chain sites. This connection was achieved using 2-(trimethylstannyl)-5-(4-(5-(trimethylstannyl)thiophen-2-ylthio)-butylthio)thiophene (TS4-Sn) flexible linkers (Fig. 14b).[173] They showed that the 2Y-wing DSMA had higher backbone planarity (dihedral angle = 38°) than the core-linked DSMA (2Y-core, dihedral angle = 83°) and end-linked DSMA (2Y-end, dihedral angle = 53°) with the same linker structures, and thus had higher electron mobility (1.49 × 10^{-4} cm^2 V^{-1} s^{-1}) and T_g (95 °C) than the 2Y-core (electron mobility = 1.09 × 10^{-5} cm^2 V^{-1} s^{-1} and T_g = 67 °C) and 2Y-end (electron mobility = 5.05 × 10^{-5} cm^2 V^{-1} s^{-1} and T_g = 85 °C). As a consequence, the D18 : 2Y-wing-based PSCs exhibited a higher PCE (17.73%) and thermal stability at 80 °C (90% PCE retention after 200 h) than the D18 : 2Y-core-based PSCs (PCE = 5.63% and 31.8% PCE retention after 200 h) and D18 : 2Y-end-based PSCs (PCE = 14.46% and 67.4% PCE retention after 200 h). Furthermore, they demonstrated that using 2Y-wing as a guest component in the D18:BS3TSe-4F host system resulted in a higher PCE of 19.13%.

3.3 Development of Y-based multimer acceptors

As end-linked OSMAs can have more than two SMA units, a broad range of end-linked multimers, such as trimers and tetramers, has been developed beyond established DSMAs (Fig. 15).[151] These multimers show even higher T_g and lower *D* values compared to SMAs and DSMAs, mainly attributed to

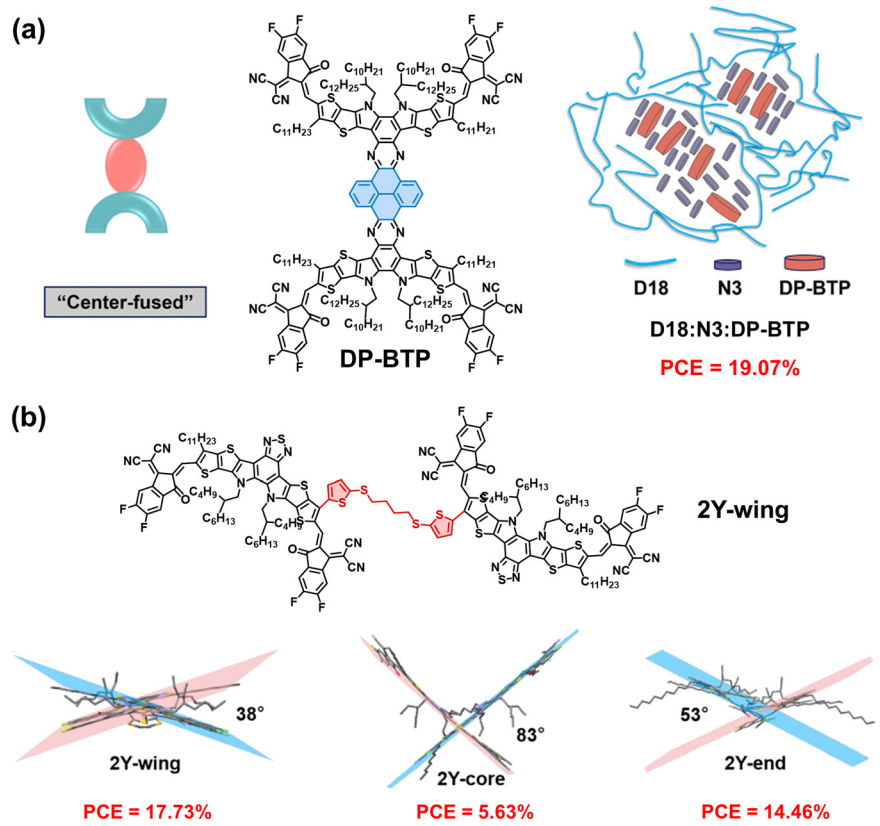

Fig. 14 DSMAs with conformations other than end-linked or core-linked structures; (a) DP-BTP and (b) 2Y-wing. Reproduced from ref. 172 and 173 with permission from the John Wiley & Sons, Inc., copyright 2024.

their larger molecular sizes that further enhance long-term stability of PSCs. In contrast, the larger molecular sizes can result in slower crystallization kinetics, which may adversely affect their crystallinity and electron mobility. As a result, the main focus in the research on Y-based multimer designs has been to identify the optimal chain lengths that balance both PCE and long-term stability of the PSCs.

The He group developed a Y-based trimer acceptor (tBTICγ-BO) by directly connecting three BT-based SMAs without any linker (Fig. 15).[70] When PM6 P_D was used, the PSCs based on tBTICγ-BO showed a slightly lower electron mobility (1.2×10^{-4} $cm^2 V^{-1} s^{-1}$) and PCE (13.16%) than DSMAs with the same backbone structure (dBTICγ-BO, electron mobility = 1.7×10^{-4} $cm^2 V^{-1} s^{-1}$ and PCE = 13.42%). This performance reduction could be due to the large dihedral angle of over 35° between the SMA units in the absence of linkers, significantly declining crystallinity as the molecular size increased.

Subsequently, our group synthesized a new trimer acceptor (TYT) using Y-SMAs and thiophene linkers to investigate the impact of molecular length on the PCE and long-term stability of the resulting PSCs (Fig. 14).[73] In this study, monomer (MYT) and dimer (DYT) acceptors with the same backbones were synthesized and their material properties were compared with the TYT acceptor to highlight the benefit of trimerization. DYT and TYT possessed relatively planar backbones as evidenced by dihedral angles between SMA units less than 16°. This molecular design allowed TYT to maintain a high electron mobility of 2.2×10^{-4} $cm^2 V^{-1} s^{-1}$, despite its larger molecular structure. In addition, the LUMO energy levels of the molecules were effectively upshifted with increasing numbers of electron-donating thiophene spacers; MYT (−4.04 eV) < DYT (−3.94 eV) < TYT (−3.86 eV), while λ_{max} of the acceptors decreased in the order of 816, 809, and 802 nm, respectively. As a result, the TYT-based PSCs produced higher V_{oc} (0.964 V) and PCE (18.15%) compared to the PSCs based on MYT (V_{oc} = 0.917 V and PCE = 16.44%) and DYT (V_{oc} = 0.942 V and PCE = 17.29%). Importantly, TYT exhibited significantly higher T_g (217 °C) compared to MYT (T_g = 80 °C) and DYT (T_g = 127 °C), due to its larger molecular size. Consequently, the D_{85} values of the acceptors decreased with increasing T_gs (and molecular size) in the order of MYT (D_{85}: 1.2×10^{-16} $cm^2 s^{-1}$), DYT (D_{85}: 1.1×10^{-19} $cm^2 s^{-1}$), and TYT (D_{85}: 1.4×10^{-25} $cm^2 s^{-1}$). Therefore, the long-term stability of the resultant PSCs under 1 sun illumination remarkably increased with chain length. Specifically, the $t_{80\%}$ lifetimes of the PM6:MYT, PM6:DYT, and PM6:TYT-based PSCs were 35, 2551, and 8454 h, respectively.

In a more recent study, the Sun group developed a new end-linked trimer acceptor with BT-based SMAs and thiophene linkers through a modified trimerization method.[151] Initially, they synthesized mono-stannylated Y-SMAs by coupling asymmetric Y-SMAs—which were difluorinated and mono-brominated at each end—with distannylated thiophenes.

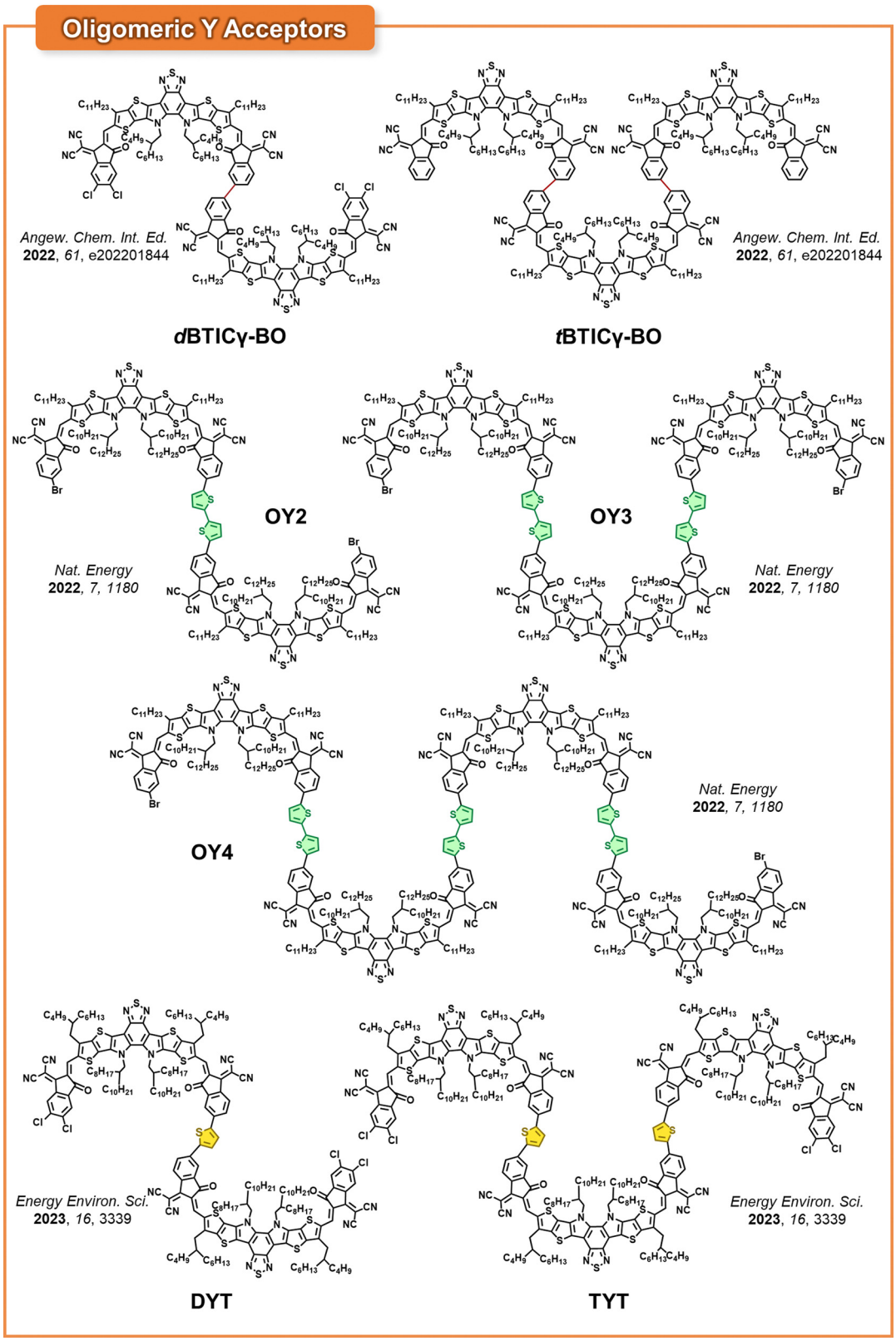

Fig. 15 Molecular structures of Y-based multimer acceptors.

Subsequently, these mono-stannylated Y-SMAs were trimerized with two dibrominated Y-SMAs to produce the trimer acceptor, Tri-Y6-OD. Intriguingly, this trimerization approach resulted in fewer by-products and simplified purification compared to

traditional end-linked trimer acceptors. They found that PSCs utilizing Tri-Y6-OD had a higher PCE of 18.03% than that (PCE = 17.46%) for the SMA based PSCs, Y6-OD. Furthermore, the Tri-Y6-OD-based PSCs displayed a significantly improved photostability under 1 sun illumination, with a $t_{80\%}$ lifetime of 1523 h, in contrast to less than 50 h for Y6-OD-based PSCs. This increased stability was attributed to the higher T_g of Tri-Y6-OD (196 °C) compared to Y6-OD (T_g = 97 °C).

In addition, Huang group devised an effective and straightforward route for the synthesis of dimer, trimer, and tetramer acceptors employing Y-SMAs and bithiophene linkers, designated as OY2, OY3, and OY4, respectively (Fig. 15).[67] They assessed the PCE and long-term stability of PSCs based on these multimers. Furthermore, they compared the results with monomer (OY1) and polymer acceptor (POY) PSCs, all of which shared identical SMA backbones with the multimers. The T_g and T_m of OY2 (T_g = 170 °C and T_m = 280 °C) and OY3 (T_g = 204 °C and T_m = 312 °C) were significantly higher than OY1 (T_g = 111 °C and T_m = 220 °C), as determined by differential scanning calorimetry (DSC). However, both OY4 and POY showed no thermal transitions, including T_g and T_m, in the DSC analysis. The absence of thermal transitions suggests that both OY4 and POY have predominantly amorphous morphologies, likely due to their slow crystallization kinetics from larger molecular sizes. As a result, the OY3-based PSCs demonstrated the highest electron mobility of 1.68×10^{-3} $cm^2 V^{-1} s^{-1}$, PCE of 14.87%, and photostability with a $t_{80\%}$ lifetime >25 000 h under 1 sun illumination among the series. Interestingly, the $t_{80\%}$ lifetime of OY3-based PSCs surpassed even that ($t_{80\%}$ lifetime = 2385 h) based on POY with longer chain lengths. The reduced all-PSC stability might be attributed to increased thermally mobile amorphous regions in the POY-based active layers consisting of polydisperse POY molecules. These observations emphasize the advantages of OSMAs with well-defined structures and suitable molecular sizes to achieve both high PCE and long-term stability in PSCs.

Recently, the development of Y-based multimer acceptors has been extended beyond traditional linear-shaped multimers. The Sun group introduced new four-arms shaped tetramers, Tet-*n* (where *n* = 0, 1, 3), incorporating flexible spacers of varying lengths – ethyl, butyl, and octyl, respectively – in their linker units (Fig. 16a).[169] To synthesize these tetramers, asymmetric Y-SMA monomers with an IC-end group on one side and a 2,5-bis(trimethylstannanyl)thiophene end group on the other were first prepared. These monomers were then connected using a tetra-brominated central core that incorporated flexible spacers of different lengths. They claimed that this method achieved higher yields (>50%) than those typically seen with conventional linear tetramer acceptors (<30%). The PSCs based on all the Tet-*n* exhibited high PCEs of 16.63–17.32%, and the PSCs based on the Tet-1 featuring butyl spacers exhibited the highest PCE (17.32%) among the series. This superior performance of Tet-1 was attributed to enhanced charge generation and reduced charge recombination, as a result of the optimal length of its flexible spacer units. Furthermore, all Tet-*n*-based PSCs showed high photostability with $t_{80\%}$ lifetimes over 1400 h under 1 sun illumination, attributed to their high T_gs exceeding 200 °C resulting from their large molecular sizes.

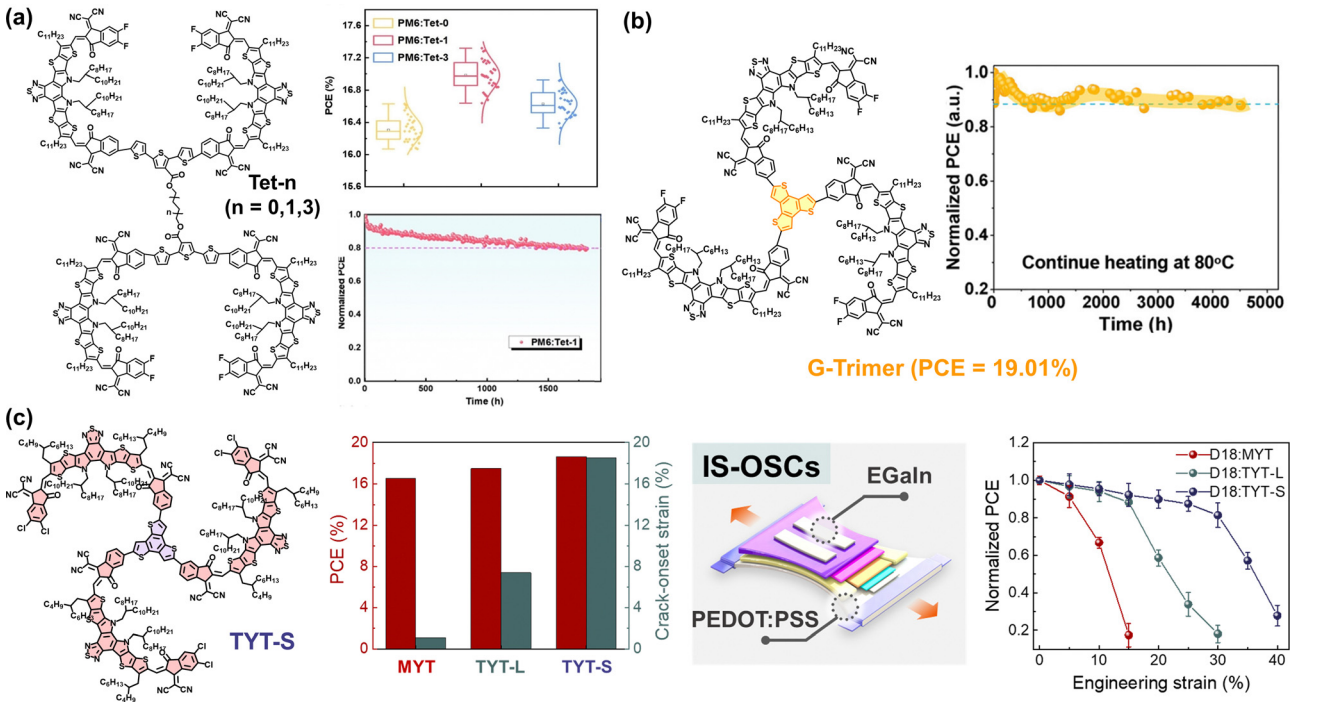

Fig. 16 Y-Based multimer acceptors beyond the conventional linear-shaped acceptors; (a) Tet-*n*, (b) G-trimer, and (c) TYT-S. Reproduced from ref. 166, 169 and 170 with permission from the John Wiley & Sons, Inc., and Elsevier B.V. copyright 2024.

Additionally, Wei group developed a new star-shaped trimer acceptor (G-trimer) using 2,5,8-tris(trimethylstannyl)benzo[1,2-*b*:3,4-*b*′:5,6-*b*″]trithiophene linkers (Fig. 16b).[166] The isotropic molecular structure of the G-trimer facilitates compact packing with low energetic disorder, enhancing charge transport efficiency. The large molecular size of the G-trimer contributes to a high T_g of 124 °C, which surpasses that of polymer (T_g = 100 °C) and dimer acceptors (T_g = 91 °C). G-trimer-based PSCs, when combined with PM6 donor and an *ortho*-xylene solution process, achieved a high PCE of 19.01% and demonstrated remarkable thermal stability at 80 °C, with a $t_{90\%}$ lifetime exceeding 4500 h. Moreover, large-area (46.2 cm^2) flexible PSCs incorporating G-trimer achieved a high PCE of 13.25%, showcasing the potential for scale-up of the oligomer acceptor-based PSCs.

Almost concurrently, our group developed a new star-shaped trimer acceptor, TYT-S (Fig. 16c).[170] The TYT-S film included a larger fraction of amorphous domains compared to the film based on linear-type trimer molecules (TYT-L) due to its isotropic molecular design. This structure promoted efficient three-dimensional charge transport in the film and enhanced charge generation at the interfaces with P_Ds in PSCs. As a result, PSCs incorporating TYT-S achieved a high PCE of 18.61%, outperforming those based on a monomer acceptor (MYT, PCE = 16.53%), as well as linear-shaped dimer (DYT, PCE = 17.20%) and TYT-L (PCE = 17.47%). In addition, the large molecular size of TYT-S contributed to a high T_g of 131 °C and significantly enhanced device photostability, with a $t_{80\%}$ lifetime of 2600 h under 1 sun illumination. Moreover, the enlarged amorphous domains and isotropic packing structure of TYT-S in the blend films played a crucial role in efficiently dissipating external mechanical stresses, which substantially increased the stretchability of active layers. This led to a COS of

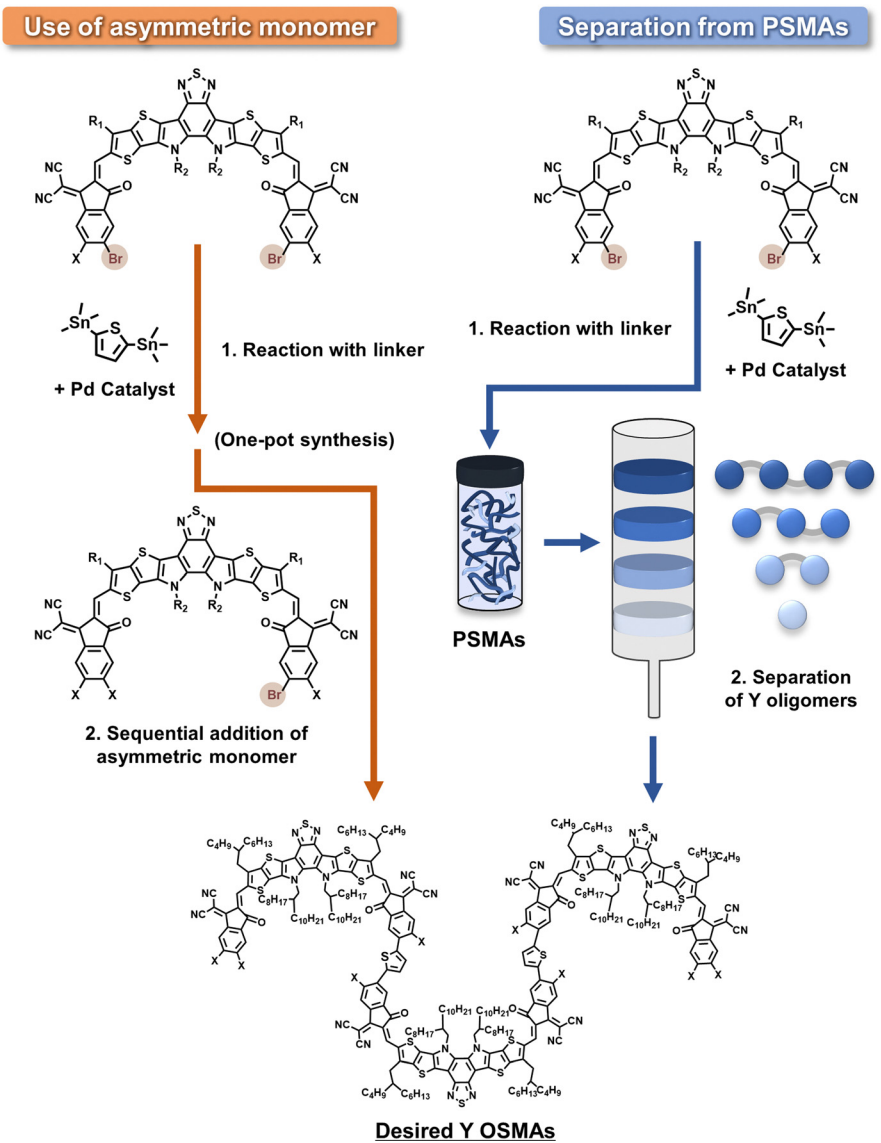

Fig. 17 Two distinct synthetic procedures for end-linked Y-based OSMAs. One involves the use of an asymmetric monomer in oligomerization (left), and the other involves the separation of the OSMAs with different lengths from the batch of PSMAs (right).

21.6% for the D18:TYT-S blend films, significantly higher than those observed with D18:MYT (COS = 1.3%) and D18:TYT-L (COS = 6.4%). Consequently, intrinsically stretchable (IS)-PSCs utilizing D18:TYT-S active layers not only achieved a high PCE of 14.4%, but also demonstrated remarkable device stretchability, retaining 80% of their PCE at a strain of 31%. This finding presents an important design guideline for the development of oligomer acceptors for efficient and mechanically robust PSCs.

3.4 Synthesis of Y-based OSMAs

The synthesis of Y-based OSMAs is more complex with a lower yield than the synthesis of SMAs and PSMAs. Two main strategies for the synthesis of end-linked OSMAs have been demonstrated. The first approach employs SMA units with asymmetric IC units employing different halogen groups at each end, specifically difluorinated (or dichlorinated) and monobrominated on either side (as shown on the left side of Fig. 16). This methodology has been utilized to synthesize end-linked OSMAs with discrete chain lengths.[71] Nevertheless, the yield for this OSMA synthetic method should be improved. The preparation of asymmetric monomers requires rigorous purification from a mixture of different SMAs with brominated or fluorinated/chlorinated on both sides, resulting in low yields ranging from 28 to 49%. Moreover, this synthesis demands stringent reaction conditions, such as maintaining a moisture and oxygen free environment for over 12 h. Consequently, the yield of the final end-linked Y-based OSMAs is typically less than 20%, substantially lower than the 30–50% yields of traditional SMAs and PSMAs[42,72]

The second synthetic approach of end-linked OSMAs was first reported by Huang group (right side of Fig. 17).[67] In this procedure, PSMAs were prepared through the Stille polycondensation between brominated Y-SMAs and stannylated linkers. Then, OSMAs with distinct chain lengths (from dimer to tetramer, denoted as OY2 to OY4) were isolated from the crude PSMA batch by column chromatography. This approach circumvents the need for synthesizing asymmetric monomers and, thus, achieves higher yields than the previous method. Specifically, di- (OY2), tri- (OY3), and tetramer (OY4) acceptors were obtained from a single PSMA batch with respective yields of 22, 23, and 30%. However, an important limitation of this synthetic method is that the obtained OSMAs are not perfectly discrete. The molecular architecture can vary depending on whether the end-capped units are linkers or IC units. Specifically, each OSMA can have three possible terminal structures: end-capped either by IC units on both sides, by linkers on both sides, or by an IC unit on one side and a linker on the other side. This structural heterogeneity in OSMAs can potentially disrupt the formation of well-ordered intermolecular assemblies and compromise electrical properties.

The synthesis of discrete core-linked OSMAs offers advantages such as low synthetic complexity and higher production yields compared to their end-linked counterparts.[159,163] This is mainly because core-linked OSMA building blocks do not require asymmetric IC end groups but necessitate bromination of the core units. As a result, the synthetic yield of core-linked OSMA monomers typically exceeds 60%, which is notably higher than end-linked OSMA yields. However, the flexibility in the molecular design of core-linked OSMAs is limited to SMA dimerization due to the inability to continuously connect more than two SMA units. This restriction poses a challenge for the development of core-linked multimer acceptors required to further enhance PSC long-term stability.

Very recently, the Zhang group demonstrated an effective method to enable the synthesis of discrete end-linked DSMAs with much improved yields.[164] First, they synthesized asymmetric monoaldehyde-terminated SMA units and coupled these with various diboronated linkers. Specifically, they employed a Lewis-acid-catalyzed Knoevenagel condensation, using boron trifluoride etherate (BF3·OEt2) as a catalyst. The preparation of these new asymmetric monomers had a higher yield under milder conditions compared to traditional end-linked DSMA synthetic strategies. As a result, an impressively high yield of 78% was achieved for the synthesis of the new DSMA named DYV.

4. Challenges and outlook for development of OSMAs

While developments in Y-based OSMAs have improved the photovoltaic performance and stability of PSCs, several challenges persist in this emerging research field. This section addresses key issues associated with (i) large-scale production, (ii) further PCE enhancement, and (iii) various stability factors of OSMA-based PSCs (Fig. 18).

4.1 Challenges for large-scale production

For the industrial adoption of OSMA-based PSCs as a renewable power source, the large-scale production cost of OSMA-based materials and devices pose a significant barrier. The majority of OSMAs are currently synthesized in small lab-scales, utilizing complex synthesis and labor-intensive purifications. Efforts to develop simple and cost-effective synthetic strategies will be invaluable. It is also essential to address the scalability in fabricating large-area devices, while ensuring environmental standards and regulation compliance.

4.1.1 Synthetic procedures for different structured OSMAs with higher yields. A grand challenge for the large-scale production of OSMA-based PSCs is the complicated synthesis and purification techniques of OSMAs. Especially, the difficult purification of monobrominated Y-SMAs from dibrominated- or difluorinated (or dichlorinated) SMAs causes end-linked OSMAs from asymmetric monomers to suffer from low synthetic yields, often less than 20%.[42,72,157] Most end-linked OSMAs have synthetic complexity (SC) indices exceeding 80–90%, which is far higher than conventional SMAs such as ITIC and Y6 (SC $<$ 70%).[184,185] Although recent promising progress on synthetic yield has been suggested by the Zhang and Sun research groups,[151,164] OSMA yields still remain substantially below conventional SMAs and PSMAs. To address these

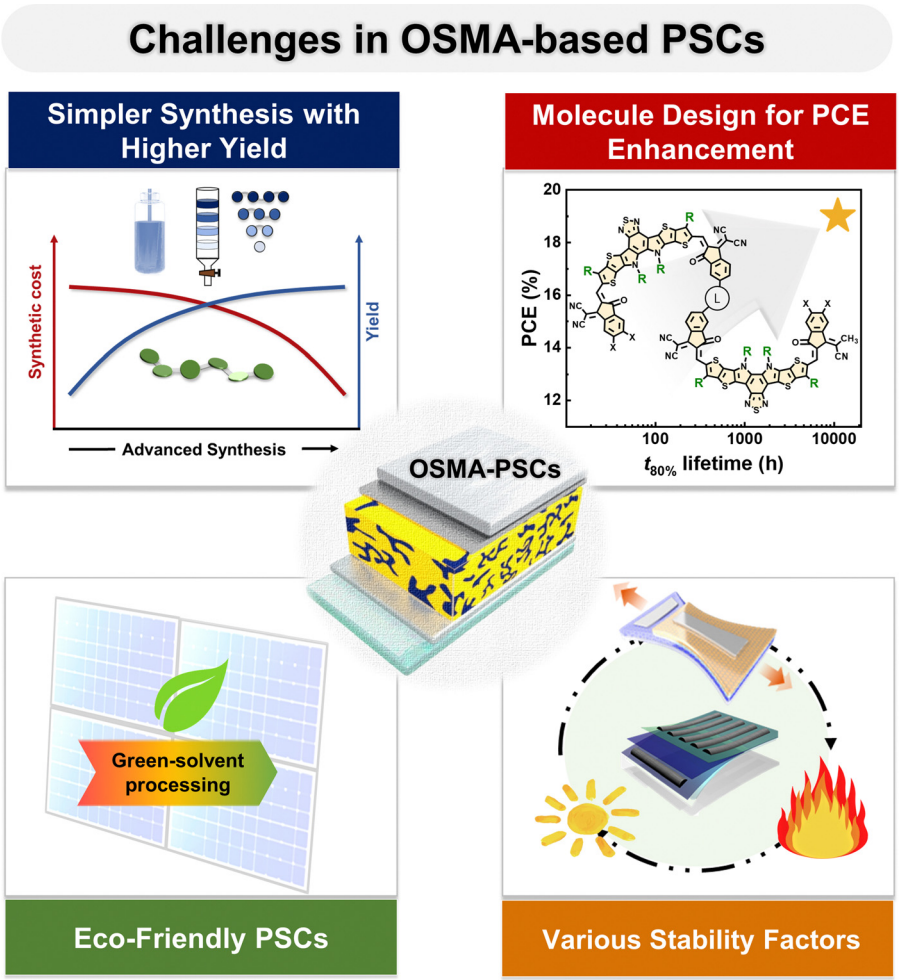

Fig. 18 Present challenges in the field of OSMA-based PSCs.

challenges, refined purification methods for the asymmetric monomers such as high-resolution chromatography are essential. Also, exploring alternative coupling processes for Y-SMAs, such as Knoevenagel or Suzuki condensation and direct arylation reactions, should be considered. In addition, end-linked OSMAs designed from structurally simple building blocks such as non-fused SMAs may be critical to minimize synthetic steps and enhance yields.

Synthetic challenges in the core-linked OSMAs also exist. Despite their higher yields compared to end-linked OSMAs, current core-linked OSMAs are predominantly limited to dimer structures because of their symmetrical molecular configurations.[159,163] This design constraint hampers the further development of advanced OSMAs, such as multimers, which can offer improved stability in PSC devices from their enlarged molecular structures. Therefore, diverse structural design of core-linked OSMA is particularly important. For example, coupling reactions of Y-SMA units *via* utilizing multi-armed linkers or linkers with multiple reactive sites can be feasible strategies to synthesize core-linked multimers.

In addition to refining synthetic protocols, it is important to optimize device fabrication by using the techniques compatible with large-scale production. Although noticeable progress has been made for large scale SMA-based PSCs (>10 cm^2) with increased PCEs above 15% by controlling crystallization kinetics of the SMAs,[186,187] similar progress should be made with OSMAs. Processing methods such as blade coating and inkjet printing can be used as scalable techniques but typically lead to poor PCE and reproducibility compared to the lab-scale spin-coating.[13,186,187] Scalable techniques necessitate use of high-boiling solvents such as chlorobenzene, which often causes excessive crystallization of the active components and non-uniform morphologies over large area.[188,189] Therefore, focused research on understanding crystallization kinetics of OSMAs during scalable printing techniques is necessary. For instance, it is essential to examine OSMA aggregation structures and crystallization kinetics during film formation, using techniques such as *in situ* UV-vis spectroscopy and *in situ* X-ray scattering.[190–193]

4.1.2 Eco-friendly processing. For large-scale production of OSMA-based PSCs, green-solvent processing is imperative.[13,194,195] However, fabrication of high-performance OSMA-based PSCs has exclusively relied on harmful halogenated solvents such as chloroform and chlorobenzene.[196] Thus, the design of side chains in

conjugated materials is crucial to enable green-solvent processing.[195,197] A main challenge is that OSMA systems possess a disadvantage in solubility as their extended molecular sizes compared to SMAs lead to poor solubility in non-halogenated solvents. Therefore, current OSMAs already incorporate long side chains (*i.e.*, 2-octyldodecyl or 2-decyltetradecyl) for good processability in halogenated solvents, restricting the adjustment of side-chain lengths for eco-friendly processing. Incorporation of longer side chains or less hydrophobic side chains (*i.e.*, ethylene glycol side chains) can ensure improved solubility in green solvents, however, it is likely to compromise crystallinity and electron mobility of the resulting OSMAs. Therefore, a careful optimization of side chain length and structure is required to balance these competing aspects.

We envision that several design strategies can be valid for obtaining green-solvent processability. First, the modification of side chains without changing length can be effective, for instance, by the introduction of functionalized side chains containing various heteroatoms.[195,198] Specifically, oxygen-containing side chains, such as siloxane or ethylene glycol, may enhance solubility in non-halogenated solvents.[199–201] Second, judicious modulation of OSMA backbone rigidity without sacrificing crystallinity can be employed. For example, the use of unfused structures or flexible functional units such as esters (–COOR) within the backbone can effectively enhance solubility in green solvent, while maintaining overall performances in devices. Finally, linker modification may endow OSMAs with good solubility.

4.2 Considerations for further PCE enhancement

As compared to SMAs, OSMAs with complex molecular structures offer more room for chemical modifications (*i.e.*, linker structure, position, regioselectivity, and modification for each SMA unit component), holding promise for further improvement in the PCEs of the PSCs. In this section, we propose potential parameters to guide the design of new OSMAs towards achieving single-junction PSCs with a PCE of 20%.

4.2.1 Achievement of high V_{oc} with reduced voltage loss. A main photovoltaic parameter limiting further PCE enhancement of SMA-based PSCs is a low V_{oc}, typically under 0.9 V.[95,96] Comparatively, OSMAs can be a more advantageous molecular platform to ensure high V_{oc} values in the PSCs, due to the inclusion of electron-donating linkers in the OSMA structure. Indeed, higher V_{oc} values (>0.9 V) in OSMA-based PSCs compared to their SMA counterparts have been demonstrated recently.[42,71,73] This advantage of OSMA-based PSCs can be fully leveraged by careful selection of electron-donating linkers, which can effectively increase V_{oc} of the resulting PSCs.[157] However, the introduction of too strong electron-donating units could result in a mismatch in the HOMO energy levels with the P_Ds, or have a negative impact on intramolecular charge transfer properties. In addition, the absorbance spectrum of the OSMAs can be blue-shifted. Hence, careful linker design with optimal electronic properties in OSMAs is critical. In addition to the linker structure, side chains, IC end groups and the core units can significantly affect various properties of OSMAs such as bandgap, LUMO energy levels, and V_{loss}.

Continued efforts on minimizing V_{loss} in OSMA-based PSCs will be crucial for higher V_{oc}. Achieving optimal blend morphology in OSMA-based PSCs can lead to low V_{loss} by reducing energetic disorders and non-radiative recombination losses.[202] A challenge in morphology optimization is to find a balance between appropriately sized, interconnected crystalline domains[203] for efficient charge transport and well-mixed donor–acceptor phases for efficient exciton dissociation. Various strategies have been explored in SMA-based PSCs to reduce V_{loss} by optimizing processing conditions including solvents, additives, and thermal/solvent annealing conditions.[202] Utilization of planar-heterojunction or pseudo bilayer type active layers was often found to be effective in minimizing energetic disorder and V_{loss} in active layers.[204,205] These strategies conducted on SMAs can be extended to achieve OSMA-based PSCs with reduced V_{loss}.

4.2.2 Enhancement of electron mobility. Despite high V_{oc} in OSMA-based PSCs, the PCE of DSMA-based PSCs is still lower than state-of-the-art SMA-based PSCs (PCE $>$ 19%), due to lower J_{sc} and FF values. This is mainly attributed to the lower electron mobility of OSMAs compared to their SMA counterparts. OSMAs composed of multiple SMA units may exhibit considerable torsion and steric hindrance between molecular building blocks, inducing less developed intermolecular assemblies and lower electron mobilities in PSCs compared to SMA-based PSCs.

To address this issue, the OSMA backbone planarity needs to be carefully controlled by a linker selection. Designing planar linkers can minimize torsion between SMA units within OSMAs, resulting in a higher electron mobility. Furthermore, the regiospecific linker placement within the OSMAs significantly impacts their molecular conformation. Additionally, the side chain length and structure, as well as introduction of functional atoms to the IC end-groups, influence the planarity and crystallinity of the OSMAs. As a result, developing OSMAs with high backbone planarity through optimum planar linker design, its regiospecific incorporation, and careful tailoring of side chains and end-groups are critical to obtaining high electron mobility and PCE in PSCs. Besides molecular design, optimization of device fabrication conditions is required to develop crystalline domains and improve electron mobility in Y-based OSMAs. For example, the use of higher boiling solvents and/or additives can be beneficial to provide sufficient crystallization times for the large OSMAs having relatively slow crystallization kinetics.

4.3 Considerations for various stability factors of OSMA-based PSCs

While OSMA-based PSCs have made notable advances in device stability under 1-sun illumination compared to SMA-based PSCs, their robustness should be further enhanced by optimizing the OSMA molecular structure. For example, beyond canonical thermal- and photo-stability testing, understanding the device performance during mechanical deformation will be

important for the practical applications of PSCs in portable and wearable electronics.

4.3.1 Optimal molecular size of OSMAs. While a variety of Y-based OSMAs have been recently developed, the optimal molecular structures and sizes to achieve the best PCE and long-term stability of the PSCs remain elusive. As recent works by He, Huang, and Kim groups have clearly shown,[67,70,73] finding optimal molecular structure/length of OSMAs is critical to obtaining the best PCE and long-term PSC stability. First, as an OSMA can be composed of a different number of SMA units (*i.e.*, dimer, trimer, and tetramer), it is essential to investigate the impact of the molecular size on both the PCE and long-term stability of the resulting PSCs. For instance, the increased molecular size of OSMAs, *via* extending the number of SMA units can lead to a rise in T_g, improving the PSC thermal stability. However, excessively large OSMAs can disrupt strong intermolecular assembly formation and decrease the electron mobility. This underlines the need for a comprehensive understanding on the relationship between the molecular structure/size and PSC performance of these OSMAs.

The investigation of the impact of molecular weight dispersity ($Đ$) on device performance and stability presents an intriguing area of research. The recent observations from the Huang and He groups demonstrate that Y-based OSMAs exhibit notably enhanced long-term PSC stability compared to PSMAs,[67,70] with extended average molecular sizes but include disperse chain lengths in a batch. These results indicate a significant influence of $Đ$ on the morphological stability of the active layer blend and the overall PSC stability. To elucidate this relationship, future research endeavors should be made by developing a model study that includes a combination of Y-based OSMAs of varied but discrete molecular lengths (*i.e.*, from monomers to pentamers).

4.3.2 Mechanical robustness for wearable applications. Despite their high PCE and long-term stability, most OSMA-based active layers in PSCs are very brittle, with COS values lower than 5%. This brittleness limits their practical applications in wearable technologies that require intrinsically stretchable component layers.[6,65,206,207] The main underlying cause of this brittleness is the rigid and planar OSMA molecular structures.[64,208] These structures, while critical for high electron mobility and T_g values, also lead to hard crystallite formation. Under mechanical stress, cracks proliferate through interfaces between these crystalline domains, ultimately compromising the mechanical robustness of the active layers.

To overcome this challenge, different strategies need to be devised. This could encompass the incorporation of highly-stretchable polymer additives to enhance the mechanical properties of the active layers.[53,209] Another promising avenue is the incorporation of flexible spacers into the OSMA backbone, which could mitigate the inherent OSMA rigidity and enhance the mechanical ductility in their films.[66,154,210] An ultimate approach could be to design OSMAs with new molecular architectures to enhance the mechanical stretchability and maintain high electron transport properties. For example, star-shaped trimer and tetramer acceptors with three-dimensional charge transport properties could be promising targets to achieve this goal.

4.3.3 Photochemical and interfacial stability. The photochemical and interfacial degradations of active materials also pose a challenge to the long-term stability of the PSCs.[10,30,211] A primary mechanism contributing to the photochemical degradation of PSCs involves the photooxidation of SMAs upon exposure to light and oxygen.[212,213] This degradation process results in modifications to the molecular structure and energy levels of SMAs containing C=C bonds, leading to the formation of hydroxyl and carbonyl groups. These transformations could elevate the incidence of C–O bonding, cause chain bond scissions, and disrupt the conjugations inside the SMA backbones.[213,214] Especially, vinyl groups linking core and IC units in SMAs can have a significant influence on their stability.[213,215] Furthermore, interfacial degradation, which can occur at the interfaces between the active layer and interlayer/electrode, is another major contributor to PSC instability.[216] Ionic interlayers such as poly(3,4-ethylenedioxythiophene):poly(styrenesulfonate) (PEDOT:PSS) are susceptible to oxidative reactions with SMAs, thereby impairing the electrical properties of the PSCs.[212] Moreover, diffusion of SMAs into these interlayers can potentially negate the long-term stability of PSCs.[217]

To address these stability issues, the following strategies can be considered in terms of molecular design of the OSMAs: first, the integration of polar functional units, such as halogens, into the OSMA backbones could amplify their quadrupole moments and facilitate stronger intermolecular interactions, thereby suppressing the photochemical reactions of C=C bonds.[218,219] Second, the design of fused-type OSMAs could potentially replace the vinyl groups connecting core and IC units, which are vulnerable to oxidation and chain scission. In addition, designing OSMAs with a high T_g and low D can suppress their diffusion to the interface and alleviate interfacial degradation.

5. Conclusions

In this article, we have reviewed the recent progress of OSMAs and highlighted key contributions that have significantly advanced the performance of OSMA-based PSCs. From the lessons from a library of OSMA literature, we also have described important guidelines for the design of efficient OSMAs and summarized their current challenges. Initially, dimer and multimer type acceptors have been conceived using PDI backbones, laying the groundwork for the current generation of ladder-type SMA-based oligomer acceptors. With the development of various Y-based OSMAs, the field has experienced remarkable advancements, including a dramatic PCE enhancement above 18% and $t_{80\%}$ lifetimes surpassing 5000 h. This success primarily stems from the discrete molecular structures and optimal chain lengths of Y-based OSMAs, leveraging the enhanced crystallinity and electron mobility of SMAs as well as the elevated T_g and restricted thermal diffusion of PSMAs. These combined features optimize PCE and long-term

stability of OSMA-based PSCs. Furthermore, we anticipate the development of new OSMA molecular design will further reduce the voltage loss and enhance electron mobility, which is crucial in improving the V_{oc}, FF, and PCE of the OSMA-based PSCs. Considering that the OSMA research field is emerging, we are optimistic that rapid advancements in design strategies will likely bring us closer to their commercial applications in the near future.

Author contributions

J.-W. Lee and J. S. Park wrote and revised the original draft. H. Jeon assisted figure drawing and collection of the statistical data. S. Lee, D. Jeong, C. Lee, and Y.-H. Kim assisted revision of the manuscript. B. J. Kim organized outline of the paper and supervised overall writings of the manuscript.

Conflicts of interest

There are no conflicts to declare.

Acknowledgements

This work was supported by the National Research Foundation of Korea (NRF-2022R1A2B5B03001761 and RS-2023-00217884).

References

1 Y. T. Hsieh, J. Y. Chen, S. Fukuta, P. C. Lin, T. Higashihara, C. C. Chueh and W. C. Chen, *ACS Appl. Mater. Interfaces*, 2018, **10**, 21712–21720.
2 Z. Jiang, K. Fukuda, W. C. Huang, S. Park, R. Nur, M. O. G. Nayeem, K. Yu, D. Inoue, M. Saito, H. Kimura, T. Yokota, S. Umezu, D. Hashizume, I. Osaka, K. Takimiya and T. Someya, *Adv. Funct. Mater.*, 2019, **29**, 1808378.
3 J. S. Park, G.-U. Kim, S. Lee, J.-W. Lee, S. Li, J.-Y. Lee and B. J. Kim, *Adv. Mater.*, 2022, **34**, 2201623.
4 J. M. Huang, Z. Lu, J. Q. He, H. Hu, Q. Liang, K. Liu, Z. W. Ren, Y. K. Zhang, H. Y. Yu, Z. J. Zheng and G. Li, *Energy Environ. Sci.*, 2023, **16**, 1251–1263.
5 J.-W. Lee, G. U. Kim, D. J. Kim, Y. Jeon, S. Li, T. S. Kim, J. Y. Lee and B. J. Kim, *Adv. Energy Mater.*, 2022, **12**, 2200887.
6 S. Seo, J.-W. Lee, D. J. Kim, D. Lee, T. N. L. Phan, J. Park, Z. P. Tan, S. Cho, T. S. Kim and B. J. Kim, *Adv. Mater.*, 2023, **35**, 2300230.
7 Z. Y. Wang, M. C. Xu, Z. L. Li, Y. R. Gao, L. Yang, D. Zhang and M. Shao, *Adv. Funct. Mater.*, 2021, **31**, 2103534.
8 J.-W. Lee, H.-G. Lee, E. S. Oh, S.-W. Lee, T. N.-L. Phan, S. Li, T.-S. Kim and B. J. Kim, *Joule*, 2024, **8**, 204–223.
9 Q. Burlingame, M. Ball and Y. L. Loo, *Nat. Energy*, 2020, **5**, 947–949.
10 P. Cheng and X. W. Zhan, *Chem. Soc. Rev.*, 2016, **45**, 2544–2582.
11 W. Y. Yang, W. Wang, Y. H. Wang, R. Sun, J. Guo, H. N. Li, M. M. Shi, J. Guo, Y. Wu, T. Wang, G. H. Lu, C. J. Brabec, Y. F. Li and J. Min, *Joule*, 2021, **5**, 1209–1230.
12 H. Yao and J. Hou, *Angew. Chem., Int. Ed.*, 2022, **61**, e202209021.
13 M. Riede, D. Spoltore and K. Leo, *Adv. Energy Mater.*, 2021, **11**, 2002653.
14 Q. Liu, Y. Jiang, K. Jin, J. Qin, J. Xu, W. Li, J. Xiong, J. Liu, Z. Xiao, K. Sun, S. Yang, X. Zhang and L. Ding, *Sci. Bull.*, 2020, **65**, 272–275.
15 J. Miao, B. Meng, Z. Ding, J. Liu and L. Wang, *J. Mater. Chem. A*, 2020, **8**, 10983–10988.
16 R. Sun, W. Wang, H. Yu, Z. Chen, X. Xia, H. Shen, J. Guo, M. Shi, Y. Zheng, Y. Wu, W. Yang, T. Wang, Q. Wu, Y. Yang, X. Lu, J. Xia, C. J. Brabec, H. Yan, Y. Li and J. Min, *Joule*, 2021, **5**, 1548–1565.
17 Z. Chen, W. Song, K. Yu, J. Ge, J. Zhang, L. Xie, R. Peng and Z. Ge, *Joule*, 2021, **5**, 2395–2407.
18 X. Yuan, Y. Zhao, D. Xie, L. Pan, X. Liu, C. Duan, F. Huang and Y. Cao, *Joule*, 2022, **6**, 647–661.
19 S. Bao, H. Yang, H. Fan, J. Zhang, Z. Wei, C. Cui and Y. Li, *Adv. Mater.*, 2021, **33**, 2105301.
20 J. Yuan, Y. Zhang, L. Zhou, G. Zhang, H.-L. Yip, T.-K. Lau, X. Lu, C. Zhu, H. Peng, P. A. Johnson, M. Leclerc, Y. Cao, J. Ulanski, Y. Li and Y. Zou, *Joule*, 2019, **3**, 1140–1151.
21 C. Yan, S. Barlow, Z. Wang, H. Yan, A. K. Y. Jen, S. R. Marder and X. Zhan, *Nat. Rev. Mater.*, 2018, **3**, 18003.
22 Y. Cui, Y. Xu, H. Yao, P. Bi, L. Hong, J. Zhang, Y. Zu, T. Zhang, J. Qin, J. Ren, Z. Chen, C. He, X. Hao, Z. Wei and J. Hou, *Adv. Mater.*, 2021, **33**, 2102420.
23 L. Zhu, M. Zhang, J. Xu, C. Li, J. Yan, G. Zhou, W. Zhong, T. Hao, J. Song, X. Xue, Z. Zhou, R. Zeng, H. Zhu, C.-C. Chen, R. C. I. MacKenzie, Y. Zou, J. Nelson, Y. Zhang, Y. Sun and F. Liu, *Nat. Mater.*, 2022, **21**, 656–663.
24 C. Li, J. Zhou, J. Song, J. Xu, H. Zhang, X. Zhang, J. Guo, L. Zhu, D. Wei, G. Han, J. Min, Y. Zhang, Z. Xie, Y. Yi, H. Yan, F. Gao, F. Liu and Y. Sun, *Nat. Energy*, 2021, **6**, 605–613.
25 F. Liu, L. Zhou, W. Liu, Z. Zhou, Q. Yue, W. Zheng, R. Sun, W. Liu, S. Xu, H. Fan, L. Feng, Y. Yi, W. Zhang and X. Zhu, *Adv. Mater.*, 2021, **33**, 2100830.
26 M. Ghasemi, H. Hu, Z. Peng, J. J. Rech, I. Angunawela, J. H. Carpenter, S. J. Stuard, A. Wadsworth, I. McCulloch, W. You and H. Ade, *Joule*, 2019, **3**, 1328–1348.
27 M. Ghasemi, N. Balar, Z. Peng, H. Hu, Y. Qin, T. Kim, J. J. Rech, M. Bidwell, W. Mask, I. McCulloch, W. You, A. Amassian, C. Risko, B. T. O'Connor and H. Ade, *Nat. Mater.*, 2021, **20**, 525–532.
28 Y. Qin, N. Balar, Z. Peng, A. Gadisa, I. Angunawela, A. Bagui, S. Kashani, J. Hou and H. Ade, *Joule*, 2021, **5**, 2129–2147.
29 Y. Li, X. Huang, K. Ding, H. K. M. Sheriff, L. Ye, H. Liu, C.-Z. Li, H. Ade and S. R. Forrest, *Nat. Commun.*, 2021, **12**, 5419.
30 L. P. Duan and A. Uddin, *Adv. Sci.*, 2020, **7**, 1903259.
31 B. C. Thompson and J. M. J. Fréchet, *Angew. Chem., Int. Ed.*, 2008, **47**, 58–77.
32 P. Cheng, Y. Li and X. Zhan, *Energy Environ. Sci.*, 2014, **7**, 2005–2011.

33 Y. He and Y. Li, *Phys. Chem. Chem. Phys.*, 2011, **13**, 1970–1983.
34 Y. He, H.-Y. Chen, J. Hou and Y. Li, *J. Am. Chem. Soc.*, 2010, **132**, 1377–1382.
35 T. Kim, J. Choi, H. J. Kim, W. Lee and B. J. Kim, *Macromolecules*, 2017, **50**, 6861–6871.
36 T. Kim, R. Younts, W. Lee, S. Lee, K. Gundogdu and B. J. Kim, *J. Mater. Chem. A*, 2017, **5**, 22170–22179.
37 P. Cheng, G. Li, X. Zhan and Y. Yang, *Nat. Photonics*, 2018, **12**, 131–142.
38 G. Zhang, J. Feng, X. Xu, W. Ma, Y. Li and Q. Peng, *Adv. Funct. Mater.*, 2019, **29**, 1906587.
39 J. Zhang, Y. Li, J. Huang, H. Hu, G. Zhang, T. Ma, P. C. Y. Chow, H. Ade, D. Pan and H. Yan, *J. Am. Chem. Soc.*, 2017, **139**, 16092–16095.
40 H. Yu, L. Arunagiri, L. Zhang, J. Huang, W. Ma, J. Zhang and H. Yan, *J. Mater. Chem. A*, 2020, **8**, 6501–6509.
41 D. Meng, D. Sun, C. Zhong, T. Liu, B. Fan, L. Huo, Y. Li, W. Jiang, H. Choi, T. Kim, J. Y. Kim, Y. Sun, Z. Wang and A. J. Heeger, *J. Am. Chem. Soc.*, 2016, **138**, 375–380.
42 C. Sun, J.-W. Lee, C. Lee, D. Lee, S. Cho, S.-K. Kwon, B. J. Kim and Y.-H. Kim, *Joule*, 2023, **7**, 416–430.
43 K. An, W. Zhong, F. Peng, W. Deng, Y. Shang, H. Quan, H. Qiu, C. Wang, F. Liu, H. Wu, N. Li, F. Huang and L. Ying, *Nat. Commun.*, 2023, **14**, 2688.
44 C. Lee, S. Lee, G.-U. Kim, W. Lee and B. J. Kim, *Chem. Rev.*, 2019, **119**, 8028–8086.
45 Z. Genene, W. Mammo, E. Wang and M. R. Andersson, *Adv. Mater.*, 2019, **31**, 1807275.
46 G. Wang, F. S. Melkonyan, A. Facchetti and T. J. Marks, *Angew. Chem., Int. Ed.*, 2019, **58**, 4129–4142.
47 H. Yan, Z. Chen, Y. Zheng, C. Newman, J. R. Quinn, F. Dötz, M. Kastler and A. Facchetti, *Nature*, 2009, **457**, 679–686.
48 B. Fan, W. Zhong, L. Ying, D. Zhang, M. Li, Y. Lin, R. Xia, F. Liu, H.-L. Yip, N. Li, Y. Ma, C. J. Brabec, F. Huang and Y. Cao, *Nat. Commun.*, 2019, **10**, 4100.
49 T. Kim, J.-H. Kim, T. E. Kang, C. Lee, H. Kang, M. Shin, C. Wang, B. Ma, U. Jeong, T.-S. Kim and B. J. Kim, *Nat. Commun.*, 2015, **6**, 8547.
50 N. Zhou and A. Facchetti, *Mater. Today*, 2018, **21**, 377–390.
51 J.-W. Lee, M. J. Sung, D. Kim, S. Lee, H. You, F. S. Kim, Y.-H. Kim, B. J. Kim and S.-K. Kwon, *Chem. Mater.*, 2020, **32**, 2572–2582.
52 Y. Zhang, Y. Xu, M. J. Ford, F. Li, J. Sun, X. Ling, Y. Wang, J. Gu, J. Yuan and W. Ma, *Adv. Energy Mater.*, 2018, **8**, 1800029.
53 J.-W. Lee, B. S. Ma, H. J. Kim, T.-S. Kim and B. J. Kim, *JACS Au*, 2021, **1**, 612–622.
54 H. You, Austin L. Jones, B. S. Ma, G.-U. Kim, S. Lee, J.-W. Lee, H. Kang, T.-S. Kim, J. R. Reynolds and B. J. Kim, *J. Mater. Chem. A*, 2021, **9**, 2775–2783.
55 Z.-G. Zhang and Y. Li, *Angew. Chem., Int. Ed.*, 2021, **60**, 4422–4433.
56 Z.-G. Zhang, Y. Yang, J. Yao, L. Xue, S. Chen, X. Li, W. Morrison, C. Yang and Y. Li, *Angew. Chem., Int. Ed.*, 2017, **56**, 13503–13507.
57 Y. Kong, Y. Li, J. Yuan and L. Ding, *InfoMat*, 2022, **4**, e12271.
58 Y. Li, J. Song, Y. Dong, H. Jin, J. Xin, S. Wang, Y. Cai, L. Jiang, W. Ma, Z. Tang and Y. Sun, *Adv. Mater.*, 2022, **34**, 2110155.
59 H. Sun, B. Liu, Y. Ma, J.-W. Lee, J. Yang, J. Wang, Y. Li, B. Li, K. Feng, Y. Shi, B. Zhang, D. Han, H. Meng, L. Niu, B. J. Kim, Q. Zheng and X. Guo, *Adv. Mater.*, 2021, **33**, 2102635.
60 H. Fu, Y. Li, J. Yu, Z. Wu, Q. Fan, F. Lin, H. Y. Woo, F. Gao, Z. Zhu and A. K. Y. Jen, *J. Am. Chem. Soc.*, 2021, **143**, 2665–2670.
61 H. Yu, Y. Wang, H. K. Kim, X. Wu, Y. Li, Z. Yao, M. Pan, X. Zou, J. Zhang, S. Chen, D. Zhao, F. Huang, X. Lu, Z. Zhu and H. Yan, *Adv. Mater.*, 2022, **34**, 2200361.
62 G. Sun, X. Jiang, X. Li, L. Meng, J. Zhang, S. Qin, X. Kong, J. Li, J. Xin, W. Ma and Y. Li, *Nat. Commun.*, 2022, **13**, 5267.
63 B. Liu, H. Sun, J.-W. Lee, J. Yang, J. Wang, Y. Li, B. Li, M. Xu, Q. Liao, W. Zhang, D. Han, L. Niu, H. Meng, B. J. Kim and X. Guo, *Energy Environ. Sci.*, 2021, **14**, 4499–4507.
64 J.-W. Lee, C. Sun, B. S. Ma, H. J. Kim, C. Wang, J. M. Ryu, C. Lim, T.-S. Kim, Y.-H. Kim, S.-K. Kwon and B. J. Kim, *Adv. Energy Mater.*, 2021, **11**, 2003367.
65 Q. Fan, W. Su, S. Chen, W. Kim, X. Chen, B. Lee, T. Liu, U. A. Méndez-Romero, R. Ma, T. Yang, W. Zhuang, Y. Li, Y. Li, T.-S. Kim, L. Hou, C. Yang, H. Yan, D. Yu and E. Wang, *Joule*, 2020, **4**, 658–672.
66 Z. Genene, J.-W. Lee, S.-W. Lee, Q. Chen, Z. Tan, B. A. Abdulahi, D. Yu, T.-S. Kim, B. J. Kim and E. Wang, *Adv. Mater.*, 2022, **34**, 2107361.
67 Y. Liang, D. Zhang, Z. Wu, T. Jia, L. Lüer, H. Tang, L. Hong, J. Zhang, K. Zhang, C. J. Brabec, N. Li and F. Huang, *Nat. Energy*, 2022, **7**, 1180–1190.
68 X. Gu, X. Zhang and H. Huang, *Angew. Chem., Int. Ed.*, 2023, e202308496.
69 M. Zhang, B. Chang, R. Zhang, S. Li, X. Liu, L. Zeng, Q. Chen, L. Wang, L. Yang, H. Wang, J. Liu, F. Gao and Z.-G. Zhang, *Adv. Mater.*, 2023, 2308606.
70 H. Wang, C. Cao, H. Chen, H. Lai, C. Ke, Y. Zhu, H. Li and F. He, *Angew. Chem., Int. Ed.*, 2022, **61**, e202201844.
71 L. Zhang, Z. Zhang, D. Deng, H. Zhou, J. Zhang and Z. Wei, *Adv. Sci.*, 2022, **9**, 2202513.
72 C. Sun, J.-W. Lee, Z. Tan, T. N.-L. Phan, D. Han, H.-G. Lee, S. Lee, S.-K. Kwon, B. J. Kim and Y.-H. Kim, *Adv. Energy Mater.*, 2023, **13**, 2301283.
73 J.-W. Lee, C. Sun, T. N.-L. Phan, D. C. Lee, Z. Tan, H. Jeon, S. Cho, S.-K. Kwon, Y.-H. Kim and B. J. Kim, *Energy Environ. Sci.*, 2023, **16**, 3339–3349.
74 F. Qi, Y. Li, R. Zhang, F. R. Lin, K. Liu, Q. Fan and A. K.-Y. Jen, *Angew. Chem., Int. Ed.*, 2023, **62**, e202303066.
75 V. D. Mihailetchi, J. K. J. van Duren, P. W. M. Blom, J. C. Hummelen, R. A. J. Janssen, J. M. Kroon, M. T. Rispens, W. J. H. Verhees and M. M. Wienk, *Adv. Funct. Mater.*, 2003, **13**, 43–46.

76 K.-H. Kim, H. Kang, H. J. Kim, P. S. Kim, S. C. Yoon and B. J. Kim, *Chem. Mater.*, 2012, **24**, 2373–2381.
77 J.-W. Lee, B. S. Ma, J. Choi, J. Lee, S. Lee, K. Liao, W. Lee, T.-S. Kim and B. J. Kim, *Chem. Mater.*, 2020, **32**, 582–594.
78 J.-W. Lee, N. Choi, D. Kim, T. N.-L. Phan, H. Kang, T.-S. Kim and B. J. Kim, *Chem. Mater.*, 2021, **33**, 1070–1081.
79 H. You, H. Kang, D. Kim, J. S. Park, J.-W. Lee, S. Lee, F. S. Kim and B. J. Kim, *ChemSusChem*, 2021, **14**, 3520–3527.
80 B. Liu, H. Sun, J.-W. Lee, Z. Jiang, J. Qiao, J. Wang, J. Yang, K. Feng, Q. Liao, M. An, B. Li, D. Han, B. Xu, H. Lian, L. Niu, B. J. Kim and X. Guo, *Nat. Commun.*, 2023, **14**, 967.
81 J. Yang, B. Xiao, A. Tang, J. Li, X. Wang and E. Zhou, *Adv. Mater.*, 2019, **31**, 1804699.
82 Y.-J. Hwang, T. Earmme, B. A. E. Courtright, F. N. Eberle and S. A. Jenekhe, *J. Am. Chem. Soc.*, 2015, **137**, 4424–4434.
83 Y.-J. Hwang, B. A. E. Courtright, A. S. Ferreira, S. H. Tolbert and S. A. Jenekhe, *Adv. Mater.*, 2015, **27**, 4578–4584.
84 Q. Tu, W. Zheng, Y. Ma, M. Zhang, Z. Li, D. Cai, P. Yin, J. Wang, S.-C. Chen, F. Liu and Q. Zheng, *CCS Chem.*, 2023, **5**, 455–468.
85 Y. Li, M. Kim, Z. Wu, C. Lee, Y. W. Lee, J.-W. Lee, Y. J. Lee, E. Wang, B. J. Kim and H. Y. Woo, *J. Mater. Chem. C*, 2019, **7**, 1681–1689.
86 C. Tang, X. Ma, J.-Y. Wang, X. Zhang, R. Liao, Y. Ma, P. Wang, P. Wang, T. Wang, F. Zhang and Q. Zheng, *Angew. Chem., Int. Ed.*, 2021, **60**, 19314–19323.
87 Y. Ma, D. Cai, S. Wan, P. Yin, P. Wang, W. Lin and Q. Zheng, *Natl. Sci. Rev.*, 2020, **7**, 1886–1895.
88 Y. Z. Lin, J. Y. Wang, Z. G. Zhang, H. T. Bai, Y. F. Li, D. B. Zhu and X. W. Zhan, *Adv. Mater.*, 2015, **27**, 1170–1174.
89 S. X. Li, C. Z. Li, M. M. Shi and H. Z. Chen, *ACS Energy Lett.*, 2020, **5**, 1554–1567.
90 G. Zhang, X.-K. Chen, J. Xiao, P. C. Y. Chow, M. Ren, G. Kupgan, X. Jiao, C. C. S. Chan, X. Du, R. Xia, Z. Chen, J. Yuan, Y. Zhang, S. Zhang, Y. Liu, Y. Zou, H. Yan, K. S. Wong, V. Coropceanu, N. Li, C. J. Brabec, J.-L. Bredas, H.-L. Yip and Y. Cao, *Nat. Commun.*, 2020, **11**, 3943.
91 F. Lin, K. Jiang, W. Kaminsky, Z. Zhu and A. K. Y. Jen, *J. Am. Chem. Soc.*, 2020, **142**, 15246–15251.
92 Y. Cui, H. F. Yao, J. Q. Zhang, K. H. Xian, T. Zhang, L. Hong, Y. M. Wang, Y. Xu, K. Q. Ma, C. B. An, C. He, Z. X. Wei, F. Gao and J. H. Hou, *Adv. Mater.*, 2020, **32**, 1908205.
93 Y. H. Cai, Y. Li, R. Wang, H. B. Wu, Z. H. Chen, J. Zhang, Z. F. Ma, X. T. Hao, Y. Zhao, C. F. Zhang, F. Huang and Y. M. Sun, *Adv. Mater.*, 2021, **33**, 2101733.
94 Z. Chen, J. Zhu, D. Yang, W. Song, J. Shi, J. Ge, Y. Guo, X. Tong, F. Chen and Z. Ge, *Energy. Environ. Sci.*, 2023, **16**, 3119–3127.
95 N. K. Elumalai and A. Uddin, *Energy Environ. Sci.*, 2016, **9**, 391–410.
96 D. Qian, Z. Zheng, H. Yao, W. Tress, T. R. Hopper, S. Chen, S. Li, J. Liu, S. Chen, J. Zhang, X.-K. Liu, B. Gao, L. Ouyang, Y. Jin, G. Pozina, I. A. Buyanova, W. M. Chen, O. Inganäs, V. Coropceanu, J.-L. Bredas, H. Yan, J. Hou, F. Zhang, A. A. Bakulin and F. Gao, *Nat. Mater.*, 2018, **17**, 703–709.
97 J.-W. Lee, C. Sun, S.-W. Lee, G.-U. Kim, S. Li, C. Wang, T.-S. Kim, Y.-H. Kim and B. J. Kim, *Energy Environ. Sci.*, 2022, **15**, 4672–4685.
98 Z. Luo, T. Liu, R. Ma, Y. Xiao, L. Zhan, G. Zhang, H. Sun, F. Ni, G. Chai, J. Wang, C. Zhong, Y. Zou, X. Guo, X. Lu, H. Chen, H. Yan and C. Yang, *Adv. Mater.*, 2020, **32**, 2005942.
99 J.-W. Lee, C. Sun, D. J. Kim, M. Y. Ha, D. Han, J. S. Park, C. Wang, W. B. Lee, S.-K. Kwon, T.-S. Kim, Y.-H. Kim and B. J. Kim, *ACS Nano*, 2021, **15**, 19970–19980.
100 T. N.-L. Phan, J.-W. Lee, E. S. Oh, S. Lee, C. Lee, T.-S. Kim, S. Li and B. J. Kim, *ACS Appl. Mater. Interfaces*, 2022, **14**, 57070–57081.
101 J.-W. Lee, J. Kim, T. H.-Q. Nguyen, D. C. Lee, Z. Tan, J. Park, T. N.-L. Phan, S. Cho and B. J. Kim, *Nano Energy*, 2024, **122**, 109338.
102 C. Sun, J.-W. Lee, S. Seo, S. Lee, C. Wang, H. Li, Z. Tan, S.-K. Kwon, B. J. Kim and Y.-H. Kim, *Adv. Energy Mater.*, 2022, **12**, 2103239.
103 Y. Cai, C. Xie, Q. Li, C. Liu, J. Gao, M. H. Jee, J. Qiao, Y. Li, J. Song, X. Hao, H. Y. Woo, Z. Tang, Y. Zhou, C. Zhang, H. Huang and Y. Sun, *Adv. Mater.*, 2023, **35**, 2208165.
104 P. Wu, Y. Duan, Y. Li, X. Xu, R. Li, L. Yu and Q. Peng, *Adv. Mater.*, 2024, **36**, 2306990.
105 T. Zhang, Y. Xu, H. Yao, J. Zhang, P. Bi, Z. Chen, J. Wang, Y. Cui, L. Ma, K. Xian, Z. Li, X. Hao, Z. Wei and J. Hou, *Energy Environ. Sci.*, 2023, **16**, 1581–1589.
106 R. Zeng, L. Zhu, M. Zhang, W. Zhong, G. Zhou, J. Zhuang, T. Hao, Z. Zhou, L. Zhou, N. Hartmann, X. Xue, H. Jing, F. Han, Y. Bai, H. Wu, Z. Tang, Y. Zou, H. Zhu, C.-C. Chen, Y. Zhang and F. Liu, *Nat. Commun.*, 2023, **14**, 4148.
107 B. Liu, W. Xu, R. Ma, J.-W. Lee, T. A. Dela Peña, W. Yang, B. Li, M. Li, J. Wu, Y. Wang, C. Zhang, J. Yang, J. Wang, S. Ning, Z. Wang, J. Li, H. Wang, G. Li, B. J. Kim, L. Niu, X. Guo and H. Sun, *Adv. Mater.*, 2023, **35**, 2308334.
108 D. Qiu, H. Zhang, C. Tian, J. Zhang, L. Zhu, Z. Wei and K. Lu, *Adv. Mater.*, 2023, **35**, 2307398.
109 W. Song, Q. Ye, S. Yang, L. Xie, Y. Meng, Z. Chen, Q. Gu, D. Yang, J. Shi and Z. Ge, *Angew. Chem., Int. Ed.*, 2023, e202310034, DOI: **10.1002/anie.202310034**.
110 X. Zhang, Z. Lu, L. Ye, C. Zhan, J. Hou, S. Zhang, B. Jiang, Y. Zhao, J. Huang, S. Zhang, Y. Liu, Q. Shi, Y. Liu and J. Yao, *Adv. Mater.*, 2013, **25**, 5791–5797.
111 Y. Lin, J. Wang, S. Dai, Y. Li, D. Zhu and X. Zhan, *Adv. Energy Mater.*, 2014, **4**, 1400420.
112 Y. Liu, C. Mu, K. Jiang, J. Zhao, Y. Li, L. Zhang, Z. Li, J. Y. L. Lai, H. Hu, T. Ma, R. Hu, D. Yu, X. Huang, B. Z. Tang and H. Yan, *Adv. Mater.*, 2015, **27**, 1015–1020.
113 Z. Luo, T. Liu, W. Cheng, K. Wu, D. Xie, L. Huo, Y. Sun and C. Yang, *J. Mater. Chem. C*, 2018, **6**, 1136–1142.
114 Y. Lin, Y. Wang, J. Wang, J. Hou, Y. Li, D. Zhu and X. Zhan, *Adv. Mater.*, 2014, **26**, 5137–5142.

115 H. Lin, S. Chen, H. Hu, L. Zhang, T. Ma, J. Y. L. Lai, Z. Li, A. Qin, X. Huang, B. Tang and H. Yan, *Adv. Mater.*, 2016, **28**, 8546–8551.
116 Z. Liu, Y. Wu, Q. Zhang and X. Gao, *J. Mater. Chem. A*, 2016, **4**, 17604–17622.
117 Akash and J. P. Tiwari, *J. Mater. Chem. C*, 2024, **12**, 838–853.
118 P. Murugan, E. Ravindran, V. Sangeetha, S.-Y. Liu and J. W. Jung, *J. Mater. Chem. A*, 2023, **11**, 26393–26425.
119 N. Liang, D. Meng and Z. Wang, *Acc. Chem. Res.*, 2021, **54**, 961–975.
120 S. Rajaram, R. Shivanna, S. K. Kandappa and K. S. Narayan, *J. Phys. Chem. Lett.*, 2012, **3**, 2405–2408.
121 J. Wang, Y. Yao, S. Dai, X. Zhang, W. Wang, Q. He, L. Han, Y. Lin and X. Zhan, *J. Mater. Chem. A*, 2015, **3**, 13000–13010.
122 H. Wang, L. Chen and Y. Xiao, *J. Mater. Chem. A*, 2017, **5**, 22288–22296.
123 H. Zhong, C.-H. Wu, C.-Z. Li, J. Carpenter, C.-C. Chueh, J.-Y. Chen, H. Ade and A. K.-Y. Jen, *Adv. Mater.*, 2016, **28**, 951–958.
124 J. Liu, S. Chen, D. Qian, B. Gautam, G. Yang, J. Zhao, J. Bergqvist, F. Zhang, W. Ma, H. Ade, O. Inganäs, K. Gundogdu, F. Gao and H. Yan, *Nat. Energy*, 2016, **1**, 16089.
125 Y. Zhong, M. T. Trinh, R. Chen, G. E. Purdum, P. P. Khlyabich, M. Sezen, S. Oh, H. Zhu, B. Fowler, B. Zhang, W. Wang, C.-Y. Nam, M. Y. Sfeir, C. T. Black, M. L. Steigerwald, Y.-L. Loo, F. Ng, X. Y. Zhu and C. Nuckolls, *Nat. Commun.*, 2015, **6**, 8242.
126 Y. Duan, X. Xu, H. Yan, W. Wu, Z. Li and Q. Peng, *Adv. Mater.*, 2017, **29**, 1605115.
127 N. Liang, K. Sun, Z. Zheng, H. Yao, G. Gao, X. Meng, Z. Wang, W. Ma and J. Hou, *Adv. Energy Mater.*, 2016, **6**, 1600060.
128 T. J. Sisto, Y. Zhong, B. Zhang, M. T. Trinh, K. Miyata, X. Zhong, X. Y. Zhu, M. L. Steigerwald, F. Ng and C. Nuckolls, *J. Am. Chem. Soc.*, 2017, **139**, 5648–5651.
129 G. Gao, N. Liang, H. Geng, W. Jiang, H. Fu, J. Feng, J. Hou, X. Feng and Z. Wang, *J. Am. Chem. Soc.*, 2017, **139**, 15914–15920.
130 H. Wang, L. Chen and Y. Xiao, *J. Mater. Chem. C*, 2017, **5**, 12816–12824.
131 S.-Y. Liu, C.-H. Wu, C.-Z. Li, S.-Q. Liu, K.-H. Wei, H.-Z. Chen and A. K.-Y. Jen, *Adv. Sci.*, 2015, **2**, 1500014.
132 W. Chen, X. Yang, G. Long, X. Wan, Y. Chen and Q. Zhang, *J. Mater. Chem. C*, 2015, **3**, 4698–4705.
133 Y. Liu, J. Y. L. Lai, S. Chen, Y. Li, K. Jiang, J. Zhao, Z. Li, H. Hu, T. Ma, H. Lin, J. Liu, J. Zhang, F. Huang, D. Yu and H. Yan, *J. Mater. Chem. A*, 2015, **3**, 13632–13636.
134 J. Lee, R. Singh, D. H. Sin, H. G. Kim, K. C. Song and K. Cho, *Adv. Mater.*, 2016, **28**, 69–76.
135 Q. Wu, D. Zhao, A. M. Schneider, W. Chen and L. Yu, *J. Am. Chem. Soc.*, 2016, **138**, 7248–7251.
136 S. Li, W. Liu, C.-Z. Li, F. Liu, Y. Zhang, M. Shi, H. Chen and T. P. Russell, *J. Mater. Chem. A*, 2016, **4**, 10659–10665.
137 D. Meng, H. Fu, C. Xiao, X. Meng, T. Winands, W. Ma, W. Wei, B. Fan, L. Huo, N. L. Doltsinis, Y. Li, Y. Sun and Z. Wang, *J. Am. Chem. Soc.*, 2016, **138**, 10184–10190.
138 K. C. Song, R. Singh, J. Lee, D. H. Sin, H. Lee and K. Cho, *J. Mater. Chem. C*, 2016, **4**, 10610–10615.
139 Q. Wu, D. Zhao, J. Yang, V. Sharapov, Z. Cai, L. Li, N. Zhang, A. Neshchadin, W. Chen and L. Yu, *Chem. Mater.*, 2017, **29**, 1127–1133.
140 A. Zhang, C. Li, F. Yang, J. Zhang, Z. Wang, Z. Wei and W. Li, *Angew. Chem., Int. Ed.*, 2017, **129**, 2738–2742.
141 X. Liu, T. Liu, C. Duan, J. Wang, S. Pang, W. Xiong, Y. Sun, F. Huang and Y. Cao, *J. Mater. Chem. A*, 2017, **5**, 1713–1723.
142 B. Wang, W. Liu, H. Li, J. Mai, S. Liu, X. Lu, H. Li, M. Shi, C.-Z. Li and H. Chen, *J. Mater. Chem. A*, 2017, **5**, 9396–9401.
143 M. Yi, J. Yi, J. Wang, L. Wang, W. Gao, Y. Lin, Q. Luo, H. Tan, C.-Q. Ma and H. Wang, *Dyes Pigm.*, 2017, **139**, 498–508.
144 H. Sun, P. Sun, C. Zhang, Y. Yang, X. Gao, F. Chen, Z. Xu, Z.-K. Chen and W. Huang, *Chem. – Asian J.*, 2017, **12**, 721–725.
145 Q. Zhang, X. Xu, S. Chen, G. B. Bodedla, M. Sun, Q. Hu, Q. Peng, B. Huang, H. Ke, F. Liu, T. P. Russell and X. Zhu, *Sustainable Energy Fuels*, 2018, **2**, 2616–2624.
146 Y. Zhao, H. Wang, S. Xia, F. Zhou, Z. Luo, J. Luo, F. He and C. Yang, *Chem. – Eur. J.*, 2018, **24**, 4149–4156.
147 H. Wang, M. Li, Y. Liu, J. Song, C. Li and Z. Bo, *J. Mater. Chem. C*, 2019, **7**, 819–825.
148 J. Zhang, F. Bai, Y. Li, H. Hu, B. Liu, X. Zou, H. Yu, J. Huang, D. Pan, H. Ade and H. Yan, *J. Mater. Chem. A*, 2019, **7**, 8136–8143.
149 G. Li, S. Wang, D. Li, T. Liu, C. Yan, J. Li, W. Yang, Z. Luo, R. Ma, X. Wang, G. Cui, Y. Wang, W. Ma, L. Huo, K. Chen, H. Yan and B. Tang, *Solar RRL*, 2020, **4**, 1900453.
150 Z. Li, Z. Zhang, H. Chen, Y. Zhang, Y.-Q.-Q. Yi, Z. Liang, B. Zhao, M. Li, C. Li, Z. Yao, X. Wan, B. Kan and Y. Chen, *Adv. Energy Mater.*, 2023, **13**, 2300301.
151 C. Zhang, J. Song, J. Xue, S. Wang, Z. Ge, Y. Man, W. Ma and Y. Sun, *Angew. Chem., Int. Ed.*, 2023, e202308595.
152 L. Ye, S. Li, X. Liu, S. Zhang, M. Ghasemi, Y. Xiong, J. Hou and H. Ade, *Joule*, 2019, **3**, 443–458.
153 Z. Wang, Z. Peng, Z. Xiao, D. Seyitliyev, K. Gundogdu, L. Ding and H. Ade, *Adv. Mater.*, 2020, **32**, 2005386.
154 J.-W. Lee, D. Jeong, D. J. Kim, T. N.-L. Phan, J. S. Park, T.-S. Kim and B. J. Kim, *Energy Environ. Sci.*, 2021, **14**, 4067–4076.
155 S. Seo, J. Kim, H. Kang, J.-W. Lee, S. Lee, G.-U. Kim and B. J. Kim, *Macromolecules*, 2021, **54**, 53–63.
156 S. E. Root, M. A. Alkhadra, D. Rodriquez, A. D. Printz and D. J. Lipomi, *Chem. Mater.*, 2017, **29**, 2646–2654.
157 J.-W. Lee, C. Sun, C. Lee, Z. Tan, T. N.-L. Phan, H. Jeon, D. Jeong, S.-K. Kwon, Y.-H. Kim and B. J. Kim, *ACS Energy Lett.*, 2023, **8**, 1344–1353.
158 S. Y. Li, R. Zhang, M. Zhang, J. Yao, Z. X. Peng, Q. Chen, C. Zhang, B. W. Chang, Y. Bai, H. Y. Fu, Y. N. Ouyang,

C. F. Zhang, J. A. Steele, T. Alshahrani, M. B. J. Roeffaers, E. Solano, L. Meng, F. Gao, Y. F. Li and Z. G. Zhang, *Adv. Mater.*, 2023, **35**, 2206563.

159 H. Chen, Z. Zhang, P. Wang, Y. Zhang, K. Ma, Y. Lin, T. Duan, T. He, Z. Ma, G. Long, C. Li, B. Kan, Z. Yao, X. Wan and Y. Chen, *Energy Environ. Sci.*, 2023, **16**, 1773–1782.

160 H. Zhuo, X. Li, J. Zhang, S. Qin, J. Guo, R. Zhou, X. Jiang, X. Wu, Z. Chen, J. Li, L. Meng and Y. Li, *Angew. Chem., Int. Ed.*, 2023, **62**, e202303551.

161 J. Wan, T. Wang, R. Sun, X. H. Wu, S. S. Wang, M. M. Zhang and J. Min, *Adv. Mater.*, 2023, **35**, 2302592.

162 J. Wu, Z. Ling, L. R. Franco, S. Y. Jeong, Z. Genene, J. Mena, S. Chen, C. Chen, C. M. Araujo, C. F. N. Marchiori, J. Kimpel, X. Chang, F. H. Isikgor, Q. Chen, H. Faber, Y. Han, F. Laquai, M. Zhang, H. Y. Woo, D. Yu, T. D. Anthopoulos and E. Wang, *Angew. Chem., Int. Ed.*, 2023, **62**, e202302888.

163 H. Chen, B. Kan, P. Wang, W. Feng, L. Li, S. Zhang, T. Chen, Y. Yang, T. Duan, Z. Yao, C. Li, X. Wan and Y. Chen, *Angew. Chem., Int. Ed.*, 2023, **62**, e202307962.

164 H. Fu, M. Zhang, Y. Zhang, Q. Wang, Z. A. Xu, Q. Zhou, Z. Li, Y. Bai, Y. Li and Z.-G. Zhang, *Angew. Chem., Int. Ed.*, 2023, **62**, e202306303.

165 M. Lv, Q. Wang, J. Zhang, Y. Wang, Z.-G. Zhang, T. Wang, H. Zhang, K. Lu, Z. Wei and D. Deng, *Adv. Mater.*, 2024, **36**, 2310046.

166 C. X. Wang, X. M. Ma, Y. F. Shen, D. Deng, H. Zhang, T. Wang, J. Q. Zhang, J. Li, R. Wang, L. L. Zhang, Q. Cheng, Z. Q. Zhang, H. Q. Zhou, C. Y. Tian and Z. X. Wei, *Joule*, 2023, **7**, 2386–2401.

167 Y. Bai, Z. Zhang, Q. Zhou, H. Geng, Q. Chen, S. Kim, R. Zhang, C. Zhang, B. Chang, S. Li, H. Fu, L. Xue, H. Wang, W. Li, W. Chen, M. Gao, L. Ye, Y. Zhou, Y. Ouyang, C. Zhang, F. Gao, C. Yang, Y. Li and Z.-G. Zhang, *Nat. Commun.*, 2023, **14**, 2926.

168 P. Tan, H. Chen, H. Wang, X. Lai, Y. Zhu, X. Shen, M. Pu, H. Lai, S. Zhang, W. Ma and F. He, *Adv. Funct. Mater.*, 2024, **34**, 2305608.

169 C. Zhang, J. L. Song, L. L. Ye, X. M. Li, M. H. Jee, H. Y. Woo and Y. M. Sun, *Angew. Chem., Int. Ed.*, 2023, **136**, e202316295.

170 J.-W. Lee, C. Sun, J. Lee, D. J. Kim, W. J. Kang, S. Lee, D. Kim, J. Park, T. N.-L. Phan, Z. Tan, F. S. Kim, J.-Y. Lee, X. Bao, T.-S. Kim, Y.-H. Kim and B. J. Kim, *Adv. Energy Mater.*, 2024, 2303872.

171 H. Jeon, K.-p Hong, J.-W. Lee, D. Jeong, T. N.-L. Phan, H.-G. Lee, J. S. Park, C. Wang, S. Xuyao, Y.-H. Kim and B. J. Kim, *Chem. Mater.*, 2023, **35**, 9276–9286.

172 X. C. Liu, Z. Zhang, C. Wang, C. F. Zhang, S. J. Liang, H. S. Fang, B. Wang, Z. Tang, C. Y. Xiao and W. W. Li, *Angew. Chem., Int. Ed.*, 2023, **136**, e202316039.

173 F. Yi, M. Xiao, Y. Meng, H. Bai, Z.-F. Yao, W. Gao, G. Qi, Z. Liang, C. Jin, L. Tang, W. Su, R. Zhang, L. Yan, Y. Liu, W. Zhu, W. Ma and Q. Fan, *Angew. Chem., Int. Ed.*, 2024, e202319295.

174 J. Yuan, T. Y. Huang, P. Cheng, Y. P. Zou, H. T. Zhang, J. L. Yang, S. Y. Chang, Z. Z. Zhang, W. C. Huang, R. Wang, D. Meng, F. Gao and Y. Yang, *Nat. Commun.*, 2019, **10**, 570.

175 J. Yuan, Y. Q. Zhang, L. Y. Zhou, C. J. Zhang, T. K. Lau, G. C. Zhang, X. H. Lu, H. L. Yip, S. K. So, S. Beaupre, M. Mainville, P. A. Johnson, M. Leclerc, H. G. Chen, H. J. Peng, Y. F. Li and Y. P. Zou, *Adv. Mater.*, 2019, **31**, 1807577.

176 Y. Cui, H. Yao, J. Zhang, T. Zhang, Y. Wang, L. Hong, K. Xian, B. Xu, S. Zhang, J. Peng, Z. Wei, F. Gao and J. Hou, *Nat. Commun.*, 2019, **10**, 2515.

177 T. L. Xu, Z. H. Luo, R. J. Ma, Z. X. Chen, T. A. Dela Pena, H. Liu, Q. Wei, M. J. Li, C. E. Zhang, J. Y. Wu, X. H. Lu, G. Li and C. L. Yang, *Angew. Chem., Int. Ed.*, 2023, **62**, e202304127.

178 Y. A. Shi, Y. L. Chang, K. Lu, Z. H. Chen, J. Q. Zhang, Y. J. Yan, D. D. Qiu, Y. A. Liu, M. A. Adil, W. Ma, X. T. Hao, L. Y. Zhu and Z. X. Wei, *Nat. Commun.*, 2022, **13**, 3256.

179 Z. Yao, X. Wan, C. Li and Y. Chen, *Acc. Mater. Res*, 2023, **4**, 772–785.

180 Z. H. Luo, T. L. Xu, C. E. Zhang and C. L. Yang, *Energy Environ. Sci.*, 2023, **16**, 2732–2758.

181 G.-U. Kim, C. Sun, J. S. Park, H. G. Lee, D. Lee, J.-W. Lee, H. J. Kim, S. Cho, Y.-H. Kim, S.-K. Kwon and B. J. Kim, *Adv. Funct. Mater.*, 2021, **31**, 2100870.

182 Y. Kim, H. Park, J. S. Park, J.-W. Lee, F. S. Kim, H. J. Kim and B. J. Kim, *J. Mater. Chem. A*, 2022, **10**, 2672–2696.

183 S. Seo, C. Sun, J.-W. Lee, S. Lee, D. Lee, C. Wang, T. N.-L. Phan, G.-U. Kim, S. Cho, Y.-H. Kim and B. J. Kim, *Adv. Funct. Mater.*, 2022, **32**, 2108508.

184 C. J. Brabec, A. Distler, X. Y. Du, H. J. Egelhaaf, J. Hauch, T. Heumueller and N. Li, *Adv. Energy Mater.*, 2020, **10**, 2001864.

185 Z. P. Yu, Z. X. Liu, F. X. Chen, R. Qin, T.-K. Lau, J. L. Yin, X. Q. Kong, X. H. Lu, M. M. Shi, C. Z. Li and H. Z. Chen, *Nat. Commun.*, 2019, **10**, 2152.

186 G. D. Wang, M. A. Adil, J. Q. Zhang and Z. X. Wei, *Adv. Mater.*, 2019, **31**, 1805089.

187 S. Park, T. Kim, S. Yoon, C. W. Koh, H. Y. Woo and H. J. Son, *Adv. Mater.*, 2020, **32**, 2002217.

188 S. Dong, T. Jia, K. Zhang, J. H. Jing and F. Huang, *Joule*, 2020, **4**, 2004–2016.

189 S. Yoon, S. Park, S. H. Park, S. Nah, S. J. Lee, J.-W. Lee, H. Ahn, H. Y. G. Yu, E. Y. Shin, B. J. Kim, B. K. Min, J. H. Noh and H. J. Son, *Joule*, 2022, **6**, 2406–2422.

190 M. Abdelsamie, K. Zhao, M. R. Niazi, K. W. Chou and A. Amassian, *J. Mater. Chem. C*, 2014, **2**, 3373–3381.

191 Y. L. Wang, X. H. Wang, B. J. Lin, Z. Z. Bi, X. B. Zhou, H. B. Naveed, K. Zhou, H. P. Yan, Z. Tang and W. Ma, *Adv. Energy Mater.*, 2020, **10**, 2000826.

192 D. Jeong, J.-W. Lee, S. Lee, G. U. Kim, H. Jeon, S. Kim, C. Yang, C. Lee and B. J. Kim, *Nano Energy*, 2023, **114**, 108618.

193 L. J. Richter, D. M. DeLongchamp and A. Amassian, *Chem. Rev.*, 2017, **117**, 6332–6366.

194 H. Y. Chen, R. Zhang, X. B. Chen, G. Zeng, L. Kobera, S. Abbrent, B. Zhang, W. J. Chen, G. Y. Xu, J. Oh, S. H. Kang, S. S. Chen, C. Yang, J. Brus, J. H. Hou, F. Gao, Y. W. Li and Y. F. Li, *Nat. Energy*, 2021, **6**, 1045–1053.
195 S. Lee, D. Jeong, C. Kim, C. Lee, H. Kang, H. Y. Woo and B. J. Kim, *ACS Nano*, 2020, **14**, 14493–14527.
196 H. Xia, Y. Zhang, W. Y. Deng, K. Liu, X. X. Xia, C. J. Su, U. S. Jeng, M. Zhang, J. M. Huang, J. W. Huang, C. Q. Yan, W. Y. Wong, X. H. Lu, W. G. Zhu and G. Li, *Adv. Mater.*, 2022, **34**, 2107659.
197 J. B. Zhao, Y. K. Li, G. F. Yang, K. Jiang, H. R. Lin, H. Ade, W. Ma and H. Yan, *Nat. Energy*, 2016, **1**, 15027.
198 S. Q. Zhang, L. Ye, H. Zhang and J. H. Hou, *Mater. Today*, 2016, **19**, 533–543.
199 J.-W. Lee, S. W. Lee, J. Kim, Y. H. Ha, C. Sun, T. N. L. Phan, S. Lee, C. Wang, T. S. Kim, Y. H. Kim and B. J. Kim, *J. Mater. Chem. A*, 2022, **10**, 20312–20322.
200 J.-W. Lee, C. Lim, S. W. Lee, Y. Jeon, S. Lee, T. S. Kim, J. Y. Lee and B. J. Kim, *Adv. Energy Mater.*, 2022, **12**, 2202224.
201 B. B. Fan, L. Ying, P. Zhu, F. L. Pan, F. Liu, J. W. Chen, F. Huang and Y. Cao, *Adv. Mater.*, 2017, **29**, 1703906.
202 Y. D. Zhang, Y. Cho, J. Lee, J. Oh, S. H. Kang, S. M. Lee, B. Lee, L. Zhong, B. Huang, S. Lee, J.-W. Lee, B. J. Kim, Y. F. Li and C. Yang, *J. Mater. Chem. A*, 2020, **8**, 13049–13058.
203 F. W. Zhao, C. R. Wang and X. W. Zhan, *Adv. Energy Mater.*, 2018, **8**, 1703147.
204 K. Jiang, J. Zhang, C. Zhong, F. R. Lin, F. Qi, Q. Li, Z. Peng, W. Kaminsky, S.-H. Jang, J. Yu, X. Deng, H. Hu, D. Shen, F. Gao, H. Ade, M. Xiao, C. Zhang and A. K. Y. Jen, *Nat. Energy*, 2022, **7**, 1076–1086.
205 L. Hong, H. Yao, Y. Cui, P. Bi, T. Zhang, Y. Cheng, Y. Zu, J. Qin, R. Yu, Z. Ge and J. Hou, *Adv. Mater.*, 2021, **33**, 2103091.
206 J.-W. Lee, T. N. L. Phan, E. S. Oh, H. G. Lee, T. S. Kim and B. J. Kim, *Adv. Funct. Mater.*, 2023, **33**, 2305851.
207 J. Lee, J.-W. Lee, H. Song, M. Song, J. Park, G.-U. Kim, D. Jeong, T.-S. Kim and B. J. Kim, *J. Mater. Chem. A*, 2023, **11**, 12846–12855.
208 J.-W. Lee, S. Seo, S. W. Lee, G. U. Kim, S. Han, T. N. L. Phan, S. Lee, S. Li, T. S. Kim, J. Y. Lee and B. J. Kim, *Adv. Mater.*, 2022, **34**, 2207544.
209 Z. X. Peng, K. H. Xian, Y. Cui, Q. C. Qi, J. W. Liu, Y. Xu, Y. B. Chai, C. M. Yang, J. H. Hou, Y. H. Geng and L. Ye, *Adv. Mater.*, 2021, **33**, 2106732.
210 Q. N. Chen, Y. H. Han, L. R. Franco, C. F. N. Marchiori, Z. Genene, C. M. Araujo, J.-W. Lee, T. N. L. Phan, J. N. Wu, D. H. Yu, D. J. Kim, T. S. Kim, L. T. Hou, B. J. Kim and E. G. Wang, *Nano-Micro Lett.*, 2022, **14**, 164.
211 M. H. Wu, B. Ma, S. S. Li, J. Q. Han and W. C. Zhao, *Adv. Funct. Mater.*, 2023, 2305445, DOI: **10.1002/adfm.202305445**.
212 M. Jorgensen, K. Norrman, S. A. Gevorgyan, T. Tromholt, B. Andreasen and F. C. Krebs, *Adv. Mater.*, 2012, **24**, 580–612.
213 Y. W. Wang, J. H. Lee, X. Y. Hou, C. Labanti, J. Yan, E. Mazzolini, A. Parhar, J. Nelson, J. S. Kim and Z. Li, *Adv. Energy Mater.*, 2021, **11**, 2003002.
214 K. Norrman, M. V. Madsen, S. A. Gevorgyan and F. C. Krebs, *J. Am. Chem. Soc.*, 2010, **132**, 16883–16892.
215 H. T. Liu, Y. B. Li, S. H. Xu, Y. H. Zhou and Z. A. Li, *Adv. Funct. Mater.*, 2021, **31**, 2106735.
216 H. L. Yip and A. K. Y. Jen, *Energy Environ. Sci.*, 2012, **5**, 5994–6011.
217 C. H. Hsieh, Y. J. Cheng, P. J. Li, C. H. Chen, M. Dubosc, R. M. Liang and C. S. Hsu, *J. Am. Chem. Soc.*, 2010, **132**, 4887–4893.
218 F. Eisner and J. Nelson, *Joule*, 2021, **5**, 1319–1322.
219 A. Markina, K.-H. Lin, W. Liu, C. Poelking, Y. Firdaus, D. R. Villalva, J. I. Khan, S. H. K. Paleti, G. T. Harrison, J. Gorenflot, W. Zhang, S. De Wolf, I. McCulloch, T. D. Anthopoulos, D. Baran, F. Laquai and D. Andrienko, *Adv. Energy Mater.*, 2021, **11**, 2102363.

